Coleman, T. A., K. R. Knupp, an P. T. Pangle, 2021: The effects of heterogeneous surface roughness on boundary-layer kinematics and wind shear. *Electronic J. Severe Storms Meteor.*, **16** (3), 1–29

Electronic Journal of
SEVERE STORMS METEOROLOGY

The Effects of Heterogeneous Surface Roughness on Boundary Layer Kinematics and Wind Shear

TIMOTHY A. COLEMAN, KEVIN R. KNUPP, and PRESTON T. PANGLE
The University of Alabama in Huntsville, Huntsville, AL

(Submitted 7 May 2021; in final form 21 December 2021)

ABSTRACT

Different types of land cover are associated with different surface roughness, which produce variations in the frictional force on the wind. Therefore, mean wind profiles at low levels often differ markedly over short distances where there is a gradient in surface roughness. Horizontal gradients in surface roughness may produce vertical vorticity, circulation, and horizontal divergence. The effect of roughness on vertical wind shear and storm-relative helicity is also qualitatively important and may lead to large gradients in helicity over short distances. Recent studies also suggest an important role of friction in tornadogenesis.

We show conceptually and theoretically how gradients in surface roughness produce quasi-ambient convergence and vertical vorticity, and gradients in vertical shear and storm-relative helicity. We then present observational data and numerical simulations that demonstrate the effects of surface roughness on the kinematics and shear of boundary-layer flow, for future work examining the importance of these processes for tornadogenesis.

1. Introduction

The continental United States east of the Rocky Mountains is characterized by a wide variety of land cover and land-use types. It is a very heterogeneous landscape, with cropland and grasslands in the Great Plains and Ohio Valley, evergreen and deciduous forests from the Southeast into the Mid-Atlantic States, and numerous bodies of water, wetlands and urban centers (Fig. 1). Such heterogeneity presents still-unsolved problems in understanding boundary-layer flows (e.g., Bou-Zeid 2020). This area is also where many U.S. tornadoes, and almost all significant (F/EF2+ rated) tornadoes, occur (e.g., Ashley 2007; Anderson-Frey and Brooks 2019).

Different types of land cover have different surface roughness as it relates to the force of friction imparted to the wind. The roughness mean wind vanishes in the logarithmic wind length (z_0) is often defined as the height where the profile (e.g., AMS 2019). The z_0 parameter is often used to quantify the effect of surface roughness on surface layer (SL) winds. The SL is often defined as the bottom 10% of the boundary layer (e.g., Geernaert 2003). The values of z_0 for different land-cover types listed in the United States Geological Survey (USGS) National Land Cover Database (NLCD) are used herein, and shown in Table 1 (e.g., Hartley et al. 2000). For a given geostrophic wind, larger values of z_0 correspond to lower SL wind speeds (e.g., Garratt 1992).

Heterogeneous land cover is typically associated with horizontal gradients in z_0. The largest z_0 gradients most commonly occur along water/land boundaries. However, large gradients in z_0 may also occur near other discontinuities in land-cover type, including those between forests, urban areas, grassland, and cropland (e.g., Garratt 1992; Grimmond and Oke 1999). Such gradients in z_0, in the presence of wind, may produce quasi-ambient (dependent on wind direction) divergence and/or vertical vorticity, acting on horizontal scales that have not been well observed.

Corresponding author address:
Dr. Timothy A. Coleman, UAH/SWIRLL, 4801 Bradford Blvd NW, Huntsville, AL 35805,
E-mail: coleman@nsstc.uah.edu

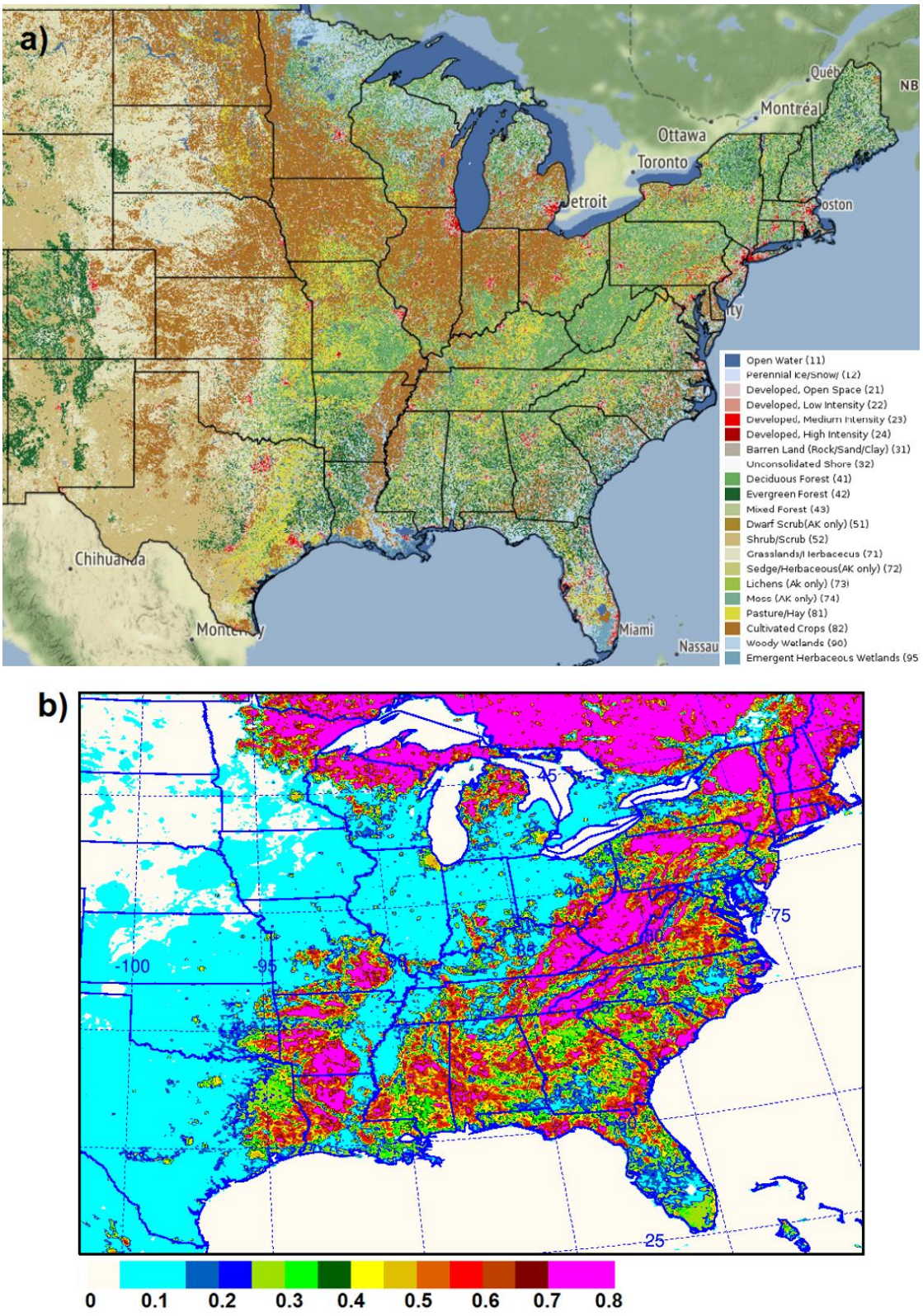

Figure 1: a) Central and eastern U.S. NLCD land-cover type (MRLC 2021); b) map of HRRR model roughness length (z_0, in m). *Click image to enlarge*.

Table 1: Roughness length (z_0) for various NLCD land-cover types.

Land Cover Type	z_0 (m)
Open water	0.001
Snow	0.012
Low residential	0.33
High residential	0.05
Commercial	0.39
Bare rock/sand	0.09
Gravel	0.18
Transitional	0.18
Deciduous forest	0.65
Evergreen forest	0.72
Mixed forest	0.71
Shrub land	0.12
Orchard/ vineyard	0.27
Grassland	0.04
Pasture	0.06
Row crops	0.06
Small grains	0.05
Fallow	0.04
Recreational grass	0.05
Woody wetland	0.55
Herbaceous wetland	0.11

In addition, the well-known log wind profile approximation (e.g., Stull 1988; Arya 1988) suggests that, in areas with increased surface roughness, there will also be an increase in vertical wind shear within the surface layer. Given the tendency of geostrophic winds to back when increased friction is present (e.g., Stull 1988), areas with higher roughness generally also have higher storm-relative helicity (SRH), a measure of the product of the storm-relative windspeed and streamwise vorticity available for tilting into the vertical in rotating storms (e.g., Davies-Jones 1984).

The objective of this paper is to introduce readers to the potential importance of surface roughness on boundary-layer divergence and convergence, vorticity, wind shear, and SRH. In some ways the paper acts as a review of well-established kinematic principles; however, it is also a research paper in that conceptual models for frictional influences on vorticity, divergence, and SRH are shown and validated using numerical models and in situ observations. Ongoing research regarding the importance of these processes to tornadogenesis will be submitted in another manuscript in the future.

Section 2 explains our datasets and methodology. In section 3, we examine the theory and kinematics of flow over heterogeneous surfaces, the divergence, circulation, and vorticity produced by such flow, and how the wind shear induced by roughness can impact storm-relative helicity. In section 4, we show observational examples of horizontal wind impacted by differential friction; we also show examples of wind profiles, near one another and with similar profiles of geostrophic wind, but with different vertical wind shear and helicity due to different z_0. In section 5, we use numerical simulations to illustrate vertical vorticity, horizontal divergence, and differences in shear and helicity, along gradients in z_0. Section 6 contains conclusions and a discussion of ongoing research.

2. Data and methodology

In analyzing observations of ambient wind flow over gradients in z_0, dual-Doppler radar analysis, using data from the Advanced Radar for Meteorological and Operational Research (ARMOR, Petersen et al. 2005), and the Mobile, AL X-band radar (MAX), are used to produce wind vectors and vorticity calculations over Lake Wheeler, AL. For the wind field over Mobile Bay, AL, Doppler radial wind velocities, in combination with velocity azimuth display (VAD) wind profiles that provide a profile of the wind direction with height, and the uniform-wind assumption (e.g., Persson and Andersson 1987; Tao 1992; Liang 2007; valid in the case herein), are used.

Observed vertical wind profiles over areas with different z_0 were determined using multiple platforms. Radiosonde data gathered during several intensive operational periods (IOPs) during the Verification of the Origin of Rotation in Tornadoes Experiment Southeast (VORTEX-SE) 2020 and 2021 field campaigns were analyzed; the sounding locations used herein were at The University of Alabama in Huntsville (UAH), and the Courtland, AL, airport (CTD, about 65 km west of UAH). Velocity azimuth display (VAD) analysis also was applied to radial velocities from the UAH Doppler Wind Lidar located at CTD to obtain vertical wind profiles at 5-min intervals, averaged over a 1-h period. Data from a Doppler sodar and a 915-MHz wind profiler, both at UAH, similarly were used to obtain wind profiles there, again using 5-min data averaged over a 1-h period.

Surface (10-m AGL) winds were added to the vertical wind profiles at all locations, including the surface berm at the UAH profiling site and the LCXA1 USCRN (Courtland 2 WSW, AL U.S. Climate Reference Network) site at CTD (both surface stations were within 250 m of the location of balloon release and instrumentation). This allowed for calculation of 0–500-m and 0–1-km SRH over areas with different z_0 that were close enough to have similar geostrophic wind profiles. SRH values at each location, calculated using the average of nearby observed storm-centroid motions, and the differences between them, were compared to those from SPC mesoanalysis (e.g., Bothwell et al. 2002; Coniglio 2012; SPC 2021) for that same time.

Land-cover maps were obtained using 2016 CONUS National Land Cover Data (NLCD), from the Multi-Resolution Land Characteristics Consortium (MRLC 2021). Numerical simulations used the High-Resolution Rapid Refresh (HRRRv3 e.g., Lee et al. 2019; NOAA 2021) model, with 3-km horizontal grid spacing. Data, some meteorological plots, and plots of HRRR roughness length were obtained from the NOAA Air Resources Laboratory (ARL 2021) Archived Meteorology site. Days for examination of the difference in winds over different z_0 in section 5c were chosen using 1-h averages of 1-min surface wind observations from Muscle Shoals, AL (KMSL), and identifying hours on non-overlapping days when average winds were roughly parallel to the long axis of Lake Wheeler, and when the wind speed was >4 m s^{-1}. Similarly, in section 5d, non-overlapping days were identified using hourly-averaged 10-m AGL winds at Little Rock, AR (KLIT), when winds were 5–6 m s^{-1}.

3. Background and theory

Flow near gradients in z_0 may produce quasi-ambient horizontal divergence and vertical vorticity, and gradients in SRH. Figure 2 shows a simple schematic of these effects along a shoreline. Surface-layer flow is slowed (and therefore backed) over higher z_0 relative to lower z_0. The process(es) through which these flow changes may affect a preexisting mesocyclone or tornado are beyond the scope of this paper, and there are additional processes, some only recently appearing in the literature, through which friction may contribute to tornadogenesis (section 6).

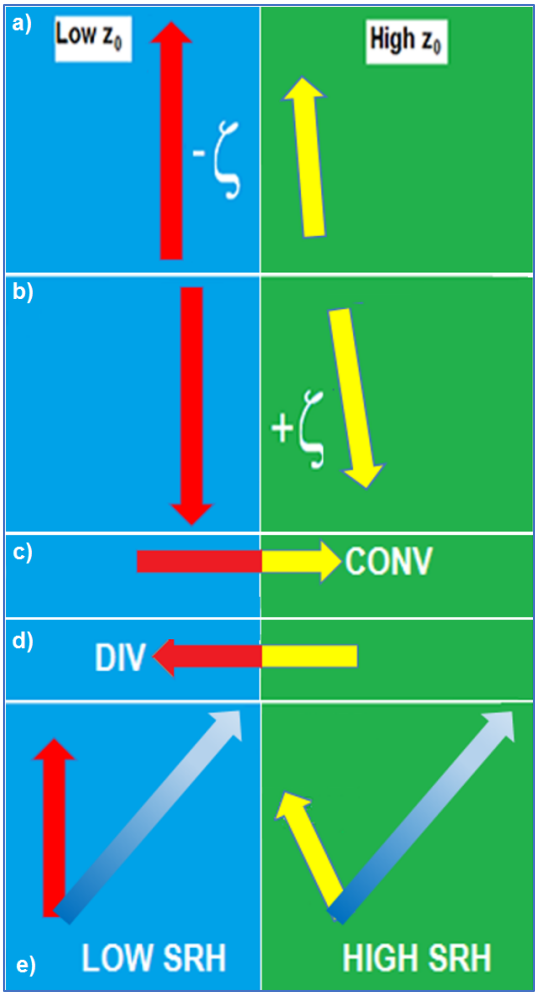

Figure 2: Schematic of vorticity, convergence, and SRH generation along a shoreline with a large gradient in z_0; a) a case where gradient in z_0 is to the right of the main surface-layer wind vector (producing negative vorticity). The colors of the solid (surface-layer) wind vectors indicate speeds (solid yellow is slow, solid red is faster by a factor of 2–3). b) As in (a), except z_0 gradient is to the left of the main wind vector (positive vorticity). c) Onshore flow (convergence). d) Offshore flow (divergence). e) Similar to surface wind in (a), but with 500-m AGL wind also shown (blue shaded vector). In each case, SL flow is slower and more backed over higher z_0. In (e) with the same 500 m AGL winds over both surfaces, the SRH is larger over greater z_0, assuming an eastward storm motion.

a. The logarithmic wind profile

The logarithmic wind profile (e.g., Tennekes 1973) is a good approximation of the profile of the mean wind in a SL with neutral stability (e.g., Stull 1988). The logarithmic wind profile may be written as

$$u(z_1) = u(z_2)\frac{\ln(\frac{z_1}{z_0})}{\ln(\frac{z_2}{z_0})} \qquad (1)$$

where z_1 and z_2 are two given heights in the SL, $u(z_1)$ and $u(z_2)$ are the mean wind speeds at those two given heights, respectively, and z_0 is roughness length. Equation 1 shows that, for a larger roughness length z_0, the ratio $u(z_1)/u(z_2)$ will be smaller, therefore wind shear will be larger in the surface layer. The effects of surface roughness, as shown below, often extend well into the BL. The instantaneous wind may deviate from Eq. 1 due to turbulence. However, Eq. 1 provides a good estimate of the profile of the mean wind in the SL and how it differs due to surface roughness.

Given a surface layer 150 m deep with a 10 m s^{-1} wind at the top of the SL, Fig. 3 shows the mean wind-speed profile, according to the logarithmic wind profile, for four different land-cover types. The wind shear between 2–150 m AGL is 0.024 s^{-1} over water, 0.037 s^{-1} over row crops, 0.048 s^{-1} over low residential, and 0.054 s^{-1} over mixed forest. Note that the low-level wind speeds are the largest over water (lowest z_0), and smallest over mixed forest (highest z_0). Also, the SL wind shear is larger in areas with higher roughness. This is consistent with the analytical expression for mean wind shear in a neutral SL, $dU/dz = u_*/kz$, that indicates the vertical shear of the mean wind U is proportional to the friction velocity u_* (which is proportional to the square root of the stress due to friction), and inversely proportional to height z and the von Karman constant k (usually near 0.4).

b. Gradients in roughness length

A geostrophic wind in the presence of horizontal gradients in roughness length leads to divergence and/or vertical vorticity, with the magnitude of each determined by the magnitude of the gradient in z_0 and the angle of the wind to that gradient. A gradient in the frictional force is listed as one of the vorticity generation terms by Bluestein (1992, E. 4.5.12, p. 249).

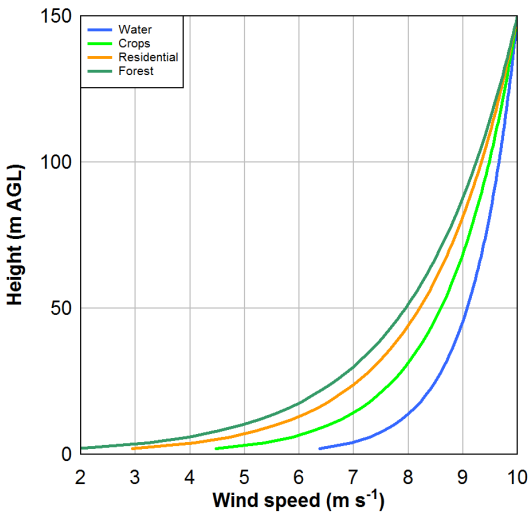

Figure 3: Windspeed profiles within a 150-m deep surface layer with a wind speed of 10 m s^{-1} at the top of the layer, for water (z_0 = 0.001 m); row crops (z_0= 0.06 m); low residential (z_0 = 0.33 m); and mixed forest (z_0 = 0.71 m). Note the smaller low-level windspeeds and larger vertical wind shear at higher z_0.

When some component of the low-level horizontal wind is normal to the gradient in z_0, quasistationary areas of horizontal shear, and associated vertical vorticity and circulation, are produced. Positive (negative) vorticity is produced when the gradient in z_0 points to the left (right) of the wind vector (Fig. 2). When some component of the low-level horizontal wind is parallel (anti-parallel) to the gradient in roughness length, convergence (divergence) is produced. These friction-related changes to the wind are mixed at least throughout the SL, and sometimes higher into the BL, producing convergence and vorticity well above the surface also. This type of vorticity and convergence production along gradients in z_0 has been discussed in other works (e.g., Welsh 2016; Kristovich et al. 2018; textbook by Rauber et al. 2019; Minder et al. 2020).

In the case of a sudden Lagrangian change in surface roughness, the wind profile does not become the log-wind profile dictated by the new z_0 instantaneously, but instead changes over a finite distance, resulting in a finite zone of convergence or divergence. A simple numerical simulation (horizontal grid spacing = 500 m), of a wind field over a mixed forest (z_0 = 0.71 m), encountering an isolated lake of open water (z_0 = 0.001 m) of finite width, is illustrated in Fig. 4.

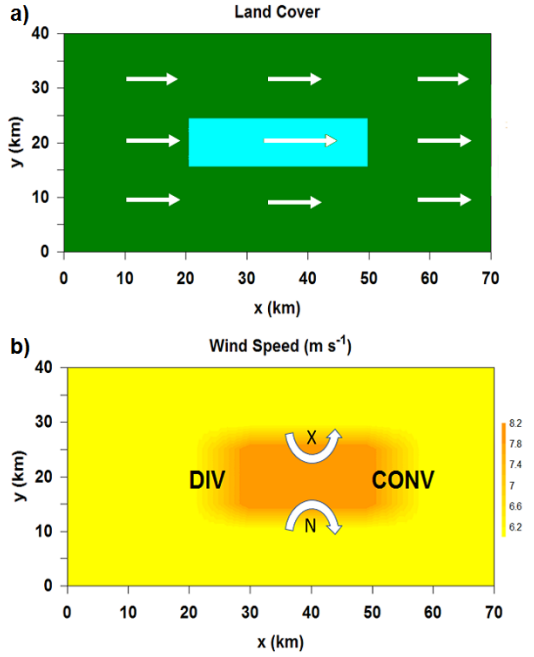

Figure 4: a) Schematic showing 10-km-wide lake (z_0 = 0.001 m) within a mixed forest (z_0 = 0.71 m). b) Map of average westerly windspeed in lowest 50 m AGL (see text). Note divergence over western end of lake, positive vorticity (and circulation) on north side of lake, and negative vorticity on south side of lake. Positive vorticity and circulation in figures throughout this paper are indicated by an "X", and negative vorticity and circulation by an "N". Divergence is indicated by "DIV", convergence by "CONV".

The same surface layer described in section 3a is applied here (depth 150 m, wind at top of SL is 10 m s^{-1}). The spatial transition in windspeeds from one z_0 to another is linear, like that parameterized in the High-Resolution Rapid Refresh (HRRR, e.g., Lee et al. 2019; NOAA 2021) model. The wind speeds shown in Fig. 4 are the average of the lowest 50 m above ground level (AGL).

The magnitude of the vorticity along a sharp gradient or discontinuity in roughness length, where the wind is blowing with some component normal to that gradient, is difficult to measure, owing to limitations in Doppler radar sample volume and smoothing in dual-Doppler analysis. Even in numerical simulations, horizontal turbulent diffusion is generally parameterized. All of these methods produce some errors in determining the distance over which the change in windspeed occurs along a gradient in z_0. However, circulation can be determined. Given the presence of friction (and possibly baroclinic effects), Kelvin's circulation theorem (e.g., Holton 1992) does not fully apply. However, given the extreme convergence associated with severe storm updrafts and mesocyclones, Kelvin's circulation theorem applies only to a useful approximation. Circulation produced by z_0 gradients, through strong convergence (e.g., in a supercell), may produce much larger magnitudes of vorticity than the magnitudes of quasi-ambient vorticity produced by gradients in friction. This is also consistent with the divergence term in the vorticity equation (e.g., Carlson 1991), and conservation of angular momentum.

c. Roughness length and storm-relative helicity

The force balance leading to the geostrophic wind is shown in Fig. 5a, where the wind achieves a direction and speed such that the pressure gradient force is balanced by the Coriolis force. However, in the boundary layer, especially in the surface layer, the force of friction, produced by surface roughness, is also large. This generally causes the wind to decelerate to subgeostrophic speeds and cross the isobars, moving from higher pressure toward lower pressure (Fig. 5b).

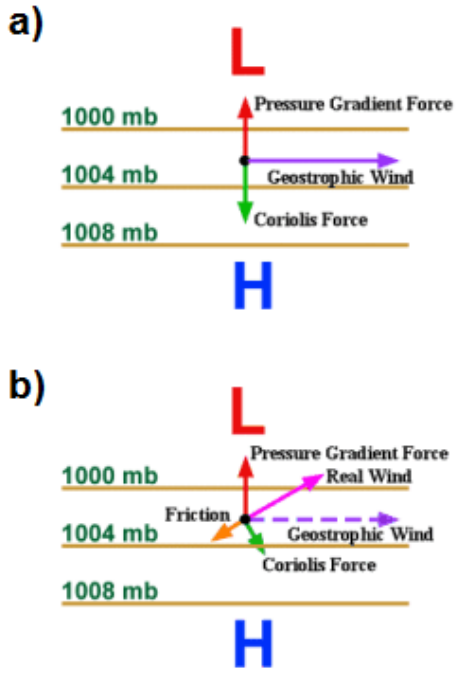

Figure 5: Force diagram for surface layer winds a) without friction and b) with friction (UIUC 2021).

The magnitude of the frictional force is roughly proportional to the roughness length. Obviously, over relatively smooth surfaces like open water (z_0 = 0.001 m), the frictional force is very small, and even SL winds are nearly geostrophic. Over much rougher surfaces with higher values of z_0, the frictional force is larger, and the SL winds are slower and directed more across the isobars (backed). As shown earlier, areas with higher surface roughness exhibit larger vertical wind shear. However, due to the cross-isobaric flow induced by the deceleration of SL winds shown in Fig. 5, there is also increased backing of winds in the SL where z_0 is larger, leading to increased veering with height over rougher surfaces because the wind speed eventually reaches geostrophic balance near the top of the boundary layer. SRH is the vertical integral of the dot product between the storm-relative wind vector and the horizontal vorticity vector (that is derived from the vertical wind shear vector). So, the combination of increased speed shear and increased veering of wind direction with height over surfaces with larger surface roughness *often leads to higher values of SRH in areas with higher values of* z_0, given a similar geostrophic wind profile.

Gentry (1983), while discussing tropical cyclone-induced tornadoes, indicated that the overland friction increase, and resulting decrease in wind speed near the surface and increase in wind shear, often results in intensification of tropical cyclone-spawned supercells as they transition from water to land. Reames and Stensrud (2018) found in numerical simulations that higher z_0 associated with an urban area caused higher SRH and more intense updraft helicity in a simulated supercell storm.

4. Ambient flow effects—Observations

In this section, observations of vorticity generation due to wind flow over large gradients in roughness length are demonstrated using both single- and dual-Doppler analysis. In addition, observed differences in storm-relative helicity, given a nearly identical geostrophic wind profile, are shown.

a. Differential friction and vorticity

1) 10 June 2008, Lake Wheeler, AL

The first example of quasi-ambient vertical vorticity comes from an experiment that was designed to observe wind perturbations associated with a lake breeze flow over Lake Wheeler in northwest Alabama, conducted by Asefi-Najafabady et al. (2010; 2012). In this example, illustrated in Fig. 6, dual-Doppler analysis was performed utilizing data from the ARMOR and MAX radars. These observations were averaged over a 1-h period. Environmental winds in the lowest 250 m AGL were from the northwest at around 5 m s^{-1}, roughly parallel to the orientation of the lake. The small vectors in Fig. 6a show the perturbation winds (from the mean flow in the lowest 250 m AGL flow over the entire domain), averaged over a 1-h period.

The average perturbation wind vectors show greater along-lake northwesterly windspeeds, with winds over the lake being as much as 4 m s^{-1} faster than those over the adjacent land, where z_0 is higher. This produced positive vorticity on the northeast side of the lake, and negative vorticity on the southwest side of the lake. This result is remarkably consistent with the simple numerical simulation shown in Fig. 4. A cross section of vertical vorticity along the orange line in the plan view analysis, at y = -11 km, illustrates that the vorticity extends above 1 km AGL. Peak values of positive vorticity are near 1.5×10^{-3} s^{-1} below 500 m AGL, but values on the order of 10^{-3} s^{-1} extend vertically above 1 km AGL. The negative vorticity on the west side was not as vigorous, but still extended to nearly 1 km AGL.

In cases such as in Fig. 6, with a lake breeze and associated upward vertical motion over the lake, some of the ambient wind shear (that is usually aligned with the wind vector), and associated horizontal vorticity, could be tilted vertically by the lake breeze, enhancing the vorticity couplet across the lake. A land breeze similarly could weaken the vorticity couplet. However, an examination of several of the cases in section 5c (not shown) indicates no significant correlation between a cooler (warmer) lake relative to land and a stronger (weaker) vorticity couplet.

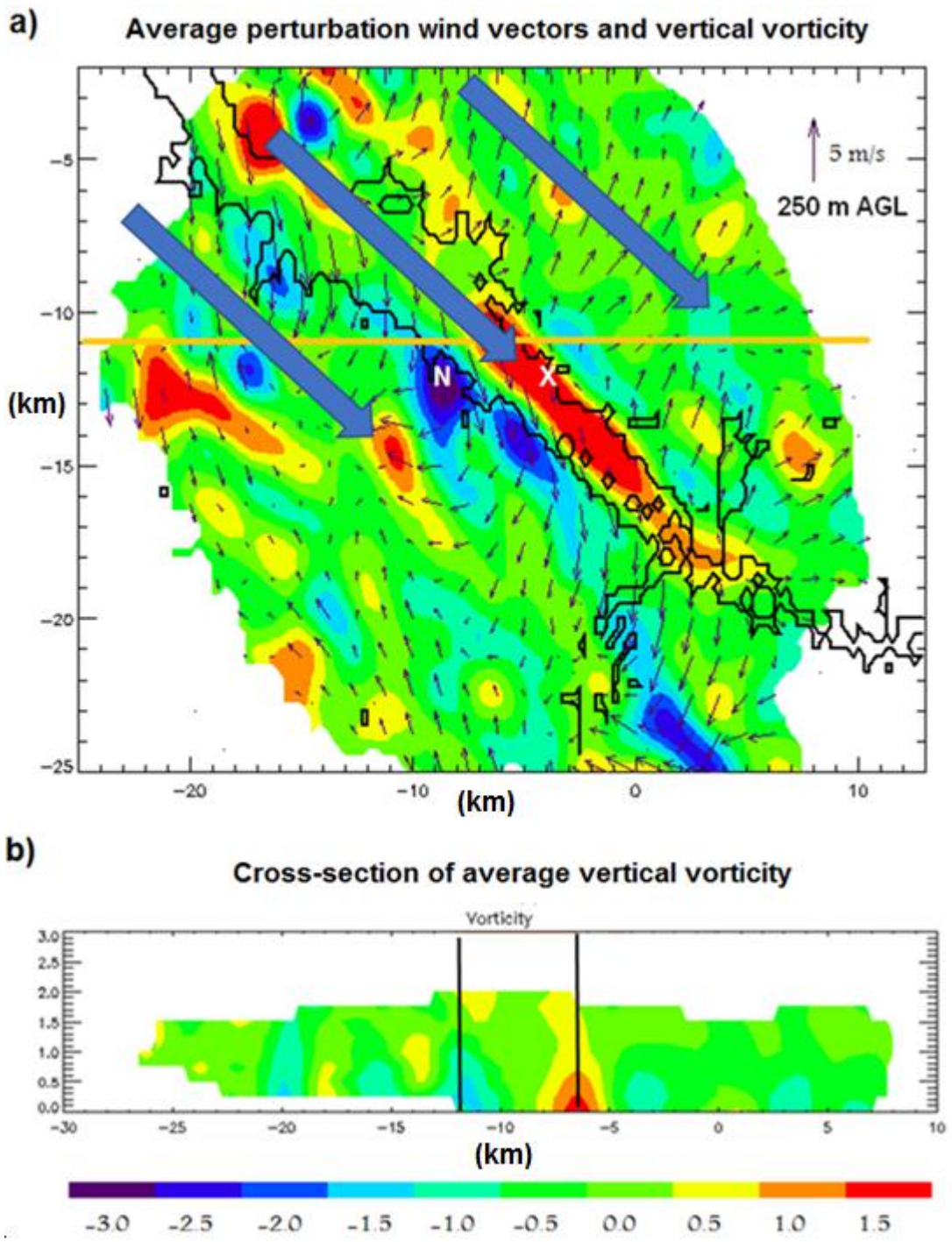

Figure 6: a) Average perturbation wind vectors (10–250 m AGL, small black) over the 1-h period 1900–2000 UTC 10 June 2008, produced by dual-Doppler analysis, over Lake Wheeler in northwest Alabama (delineated by black borders). Note the positive northwesterly perturbation winds over the lake (i.e., winds faster than the average background wind from the NW, shown by large blue arrows). Vertical vorticity is color shaded, in units of 10^{-3} s^{-1}. Enhanced winds over the lake produced positive vorticity on its north side and negative vorticity on the south side. b) Vertical cross section of vertical vorticity at y = –11 km (along orange line in (a), where vertical lines represent lake boundaries at y = –11 km. Adapted from Asefi-Najafabady et al. (2010). Distances are relative to the Mobile, AL X-band radar (MAX). ARMOR was 122°, 18 km from MAX.

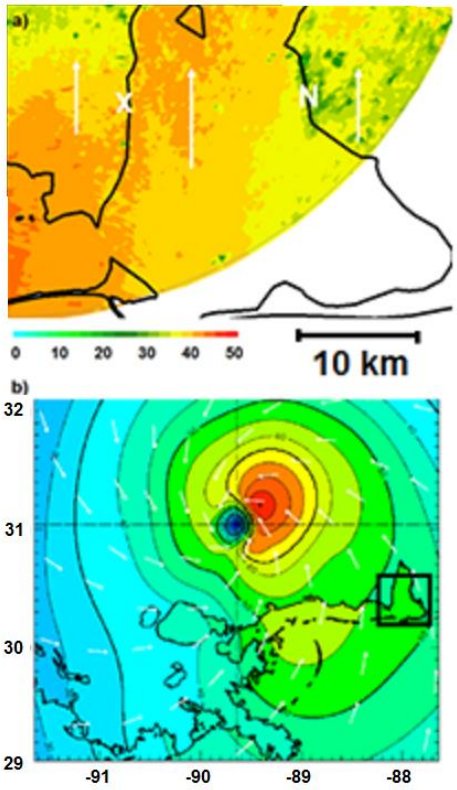

Figure 7: a) 1-h average wind speed (m s^{-1}) at 0.5° elevation from the KMOB WSR-88D, over Mobile Bay, 1759–1859 UTC 29 August 2005. b) AOML 1-min sustained surface wind map and vectors for Hurricane Katrina at 1800 UTC 29 August 2005. The black box in (b) represents the domain in panel (a).

2) 29 August 2005, Mobile Bay, AL

A second example occurred on 29 August 2005 over Mobile Bay, AL, during Hurricane Katrina. The method used to produce average wind speeds using radial velocity data and VAD wind profiles is described in section 2. Data from 1759–1859 UTC from the Mobile, AL (KMOB) WSR-88D were averaged to approximate winds over coastal Alabama (Fig. 7a). Relatively uniform south-southeasterly flow was in place over Mobile Bay, about 200 km southeast of Katrina's center (Fig. 7b). The radar provided data across most of the domain shown in Fig. 7a between 250 and 500 m AGL. Note the higher windspeeds, generally ≥40 m s^{-1}, over the water (the Gulf of Mexico and Mobile Bay), and lower (<35 m s^{-1}) over the rougher land on both sides of the bay, where z_0 is larger. This created positive quasi-ambient vorticity on the western shore of Mobile Bay on the order of 10^{-2} s^{-1}, like the magnitude of the vorticity in a mesocyclone, and negative vorticity on the eastern shore.

b. Differences in SRH over different z_0

As discussed in section 3c, when two locations have an equivalent geostrophic wind profile but different z_0, the location with higher z_0 should have larger low-level vertical wind shear and SRH. This is partly due to the slowing of near-surface winds over higher z_0. On 28 days in 2016, the average wind direction at UAH was southerly (150–210°), and the average wind speed was >2 m s^{-1}. The UAH surface station is in an urban area (HRRR z_0 = 0.41 m). Surface wind data from UAH, and from the KHSV ASOS, located in an open airport location (HRRR z_0 = 0.24 m), surrounded by grassland, but only 235°, 15 km from UAH, were gathered for these 28 days and averaged over 15-min non-overlapping intervals. This allowed for a total of 2688 15-min intervals for 10-m windspeed comparison.

Figure 8 shows scatterplots comparing the wind speeds and directions at these two locations. Figure 8a clearly shows that the winds at KHSV are higher, with 96% of the points above the $y = x$ perfect-correlation line. On average, the KHSV wind speed (lower z_0) was 1.8 m s^{-1} larger than at UAH (higher z_0). Figure 8b is inconclusive regarding the expected backing of wind direction at UAH. The wind direction at UAH was less than that at KHSV (indicating backing at UAH) only 46% of the time. That number increases to 55% of time when winds at KHSV were >5 m s^{-1} (not shown), but still there is no definitive indication of backing due to the slower winds at UAH in this dataset. Wind direction is subject to calibration errors of as much as 5°.

Next, radiosonde data, in addition to DWL, 915-MHz profiler, and Doppler sodar data (at 5 min resolution, averaged over 1 h) from CTD and UAH from VORTEX SE IOPs were used to compare wind shear and SRH (see section 2). CTD is 65 km west-southwest of UAH, in a large, open airport location (HRRR z_0 = 0.27 m) with grassland and cultivated crops 1.6 km upwind (for southerly winds). Like KHSV, CTD is in a region with a lower surface roughness than UAH. Data were examined only from IOPs when the 0–1-km SRH was positive, and no deep convection was affecting either site. Two caveats

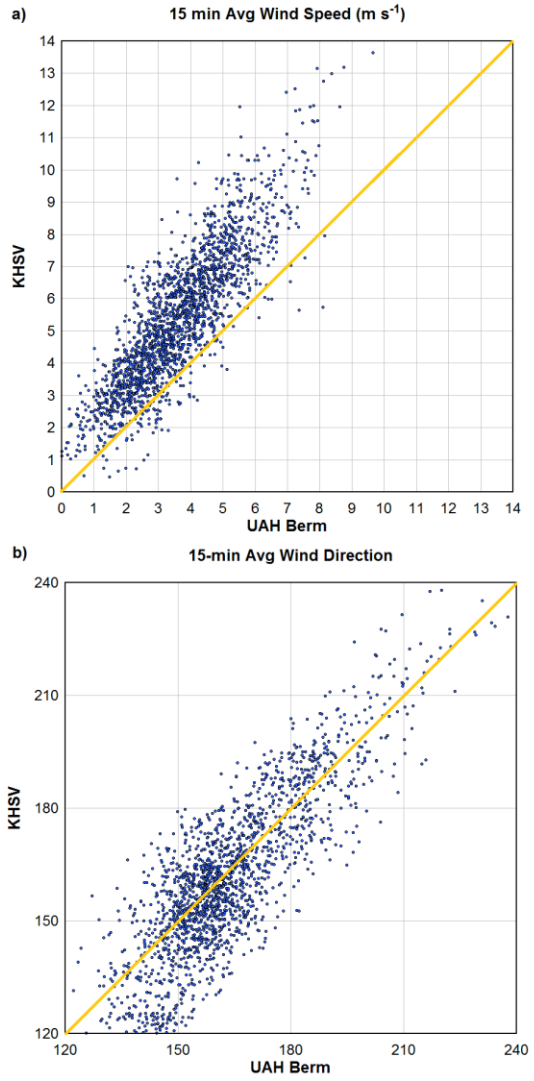

Figure 8: Scatterplot showing a) 10-m AGL windspeed and b) 10-m AGL wind direction at UAH Berm (x-axis) and KHSV (y-axis) for the 15-min intervals described in the text, and the *y* = *x* perfect-correlation line.

should be noted regarding the following examples: a) it is possible that some processes at spatial scales smaller than the SPC mesoanalysis can resolve may affect SRH, and b) as discussed by Markowski and Richardson (2007) in summertime convective BLs, some heterogeneities in SRH occur in the absence of any gradients in friction or thermal boundaries. However, the consistency of the differences found in these examples indicates the likelihood of frictional influences.

The first comparison was from VSE IOP 4, on 5 February 2020. As shown in Fig. 9a, SPC mesoanalysis at 2200 UTC indicates similar 0–1-km SRH at CTD and UAH. The average surface (10 m AGL) wind at CTD during 2100–2200 UTC was from 183° at 4 m s^{-1}, while at UAH it was from 169° at 3.4 m s^{-1}. This shows a slight slowing and backing of the surface winds at UAH. The 1-h average 0–500 m AGL SRH (e.g., Coffer et al. 2019) was 135 m^2 s^{-2} at CTD and 163 m^2 s^{-2} over the rougher surface at UAH, consistent with section 3c (Fig. 9b,c). 0–1-km SRH at 2200 UTC (not shown) was 202 m^2 s^{-2} at CTD and 250 m^2 s^{-2} at UAH; most of this difference is due to the slowed and backed surface winds at UAH.

A comparison of wind profiles at 1700 UTC from VSE IOP 11, on 23 April 2020, also was performed (not shown). In this case, SPC mesoanalysis indicated a west-to-east gradient in 0–1-km SRH at 1700 UTC that would have resulted in a 0-1-km SRH value about 75 m^2 s^{-2} higher at UAH than at CTD. However, radiosonde data from those two locations at 1700 UTC indicate 0-1-km SRH of 156 m^2 s^{-2} at CTD and 342 m^2 s^{-2} at UAH, a much greater difference of 186 m^2 s^{-2}. This is consistent with additional effects of the smoother surface causing the much lower SRH at CTD than at UAH. The 1-h average surface wind between 1630 and 1730 UTC at CTD was from 181° at 5.5 m s^{-1}, while at UAH it was from 154° at 3.8 m s^{-1}. SPC mesoanalysis (not shown) indicates no thermal, pressure, or wind- shift boundaries between CTD and UAH at 1700 UTC. Again, surface winds at UAH likely were backed and slowed due to higher z_0. The 1-h average 0–500 m AGL SRH, between 1630 and 1730 UTC, was 130 m^2 s^{-2} at CTD, and 187 m^2 s^{-2} over the rougher surface at UAH.

Finally, all simultaneous radiosonde pairs that were not contaminated by convection or thermal boundaries, from the two VSE IOPs discussed above (5 February 2020 and 23 April 2020), in addition to a pre-QLCS IOP conducted on 27–28 March 2021, were compared for 0–1-km SRH at CTD vs. UAH. Twelve radiosondes were released (nearly) simultaneously at UAH and CTD during these three IOPs without convective contamination. What can be inferred from a small sample size like this is limited, but the information is useful and consistent with section 3c. A scatterplot of the 0–1-km SRH for these 24 total soundings is shown in Fig. 10. The y-intercept of the best-fit line was 94 m^2 s^{-2}. Even with a slope of 0.76 (indicating that the

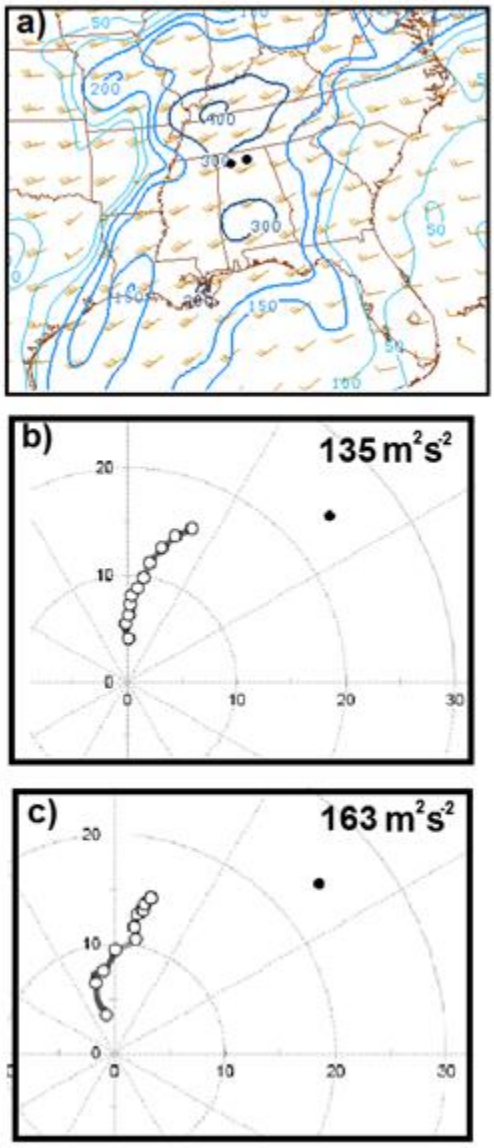

Figure 9: a) SPC mesoanalysis of 0–1-km SRH at 2200 UTC 5 February 2020. Hodographs of 1-h average 0–500-m AGL winds and SRH from 2100 through 2200 UTC at b) CTD and c) UAH. Speeds are shown in m s^{-1}. The two dots in panel (a) indicate the locations of CTD (left) and UAH (right). Black dot shows observed storm motion.

difference between the two stations decreased at higher SRH), the 0–1-km SRH was, on average 46 m^2 s^{-2} higher at UAH than at CTD, and the SRH was equal to or higher at UAH than CTD in 9 of 12 simultaneous sounding pairs.

While some of the difference in SRH may be attributed to different vertical profiles of the

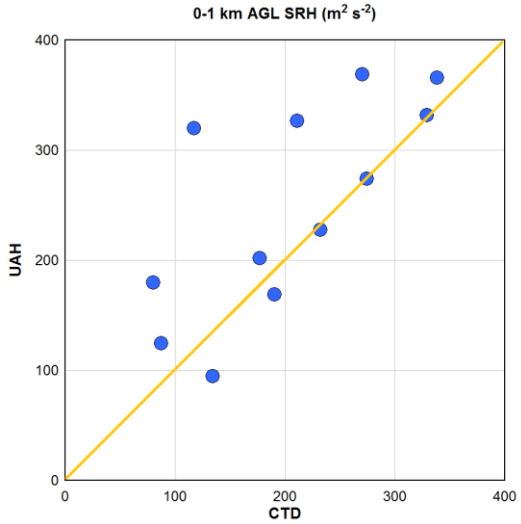

Figure 10: Scatterplot of 0–1-km SRH at CTD (x-axis) vs. UAH (y-axis) for simultaneous soundings at 12 different times during the three VSE IOPs listed in the text. Orange line is one-to-one fit.

pressure gradient, this was not the only cause. HRRR model 850- hPa winds (and specifically the position of the low-level jet, as a reviewer recommended) for all 12 times showed no definitive evidence that the differences in SRH were caused only by differences in the low-level geostrophic wind field.

5. Examples from HRRR simulations

Operational HRRR simulations show the effects of surface roughness on SL windspeeds, and the resulting low-level vorticity and convergence. In addition, the HRRR resolves higher storm relative helicity values over rougher terrain in similar gradient wind profiles. Several examples of such numerical simulations follow. The roughness length z_0 in the HRRR, for the United States east of the Rockies, is shown in Fig. 1b.

a. Florida Panhandle coastline

Hurricane Sally made landfall near Gulf Shores, AL, on 16 September 2020 at 0945 UTC, as a Category 2 storm (NHC 2020a). The cyclone then weakened as it moved slowly northeastward across Alabama, Georgia, and South Carolina on 16–17 September. Just after landfall, at 1200 UTC 16 September (Fig. 11a), the circulation around Hurricane Sally was producing southeasterly winds along the coast of the Florida Panhandle. The surface (10-m AGL)

flow at 1200 UTC, along the area of coastline near Panama City Beach, FL, including St. Andrew's Bay, was examined using the HRRR model. This is shown in Fig. 11b.

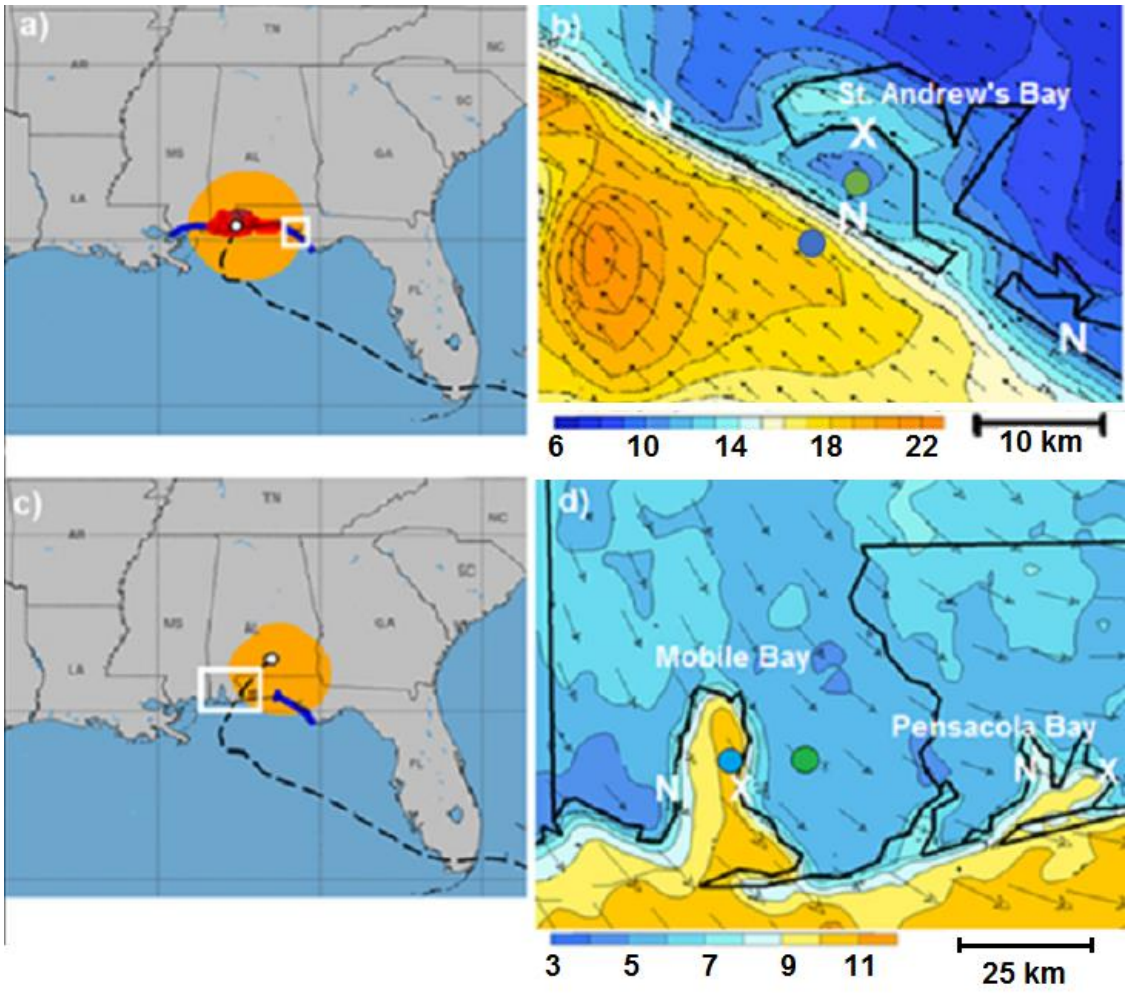

Figure 11: a) Past track (dashed) and current position (white dot) of the center of Hurricane Sally, and wind field (tropical storm winds in orange, hurricane winds in red) at 1200 UTC 16 Sep 2020 (NHC 2020b); b) HRRR 10-m wind vectors and 1 m s^{-1} windspeed contours near Panama City Beach, FL, at 1200 UTC 16 September 2020. Coastline shown in heavy black; study region for (b) shown by white square in (a); blue and green dots show locations of water vs. land wind and bulk wind difference locations referred to in text; c) Track, position, and wind field information as in (a) but at 0000 UTC 17 Sep 2020 (NHC 2020b); d) HRRR 10-m wind vectors and windspeed contours (m s^{-1}) near Mobile Bay, AL, at 0100 UTC 17 September 2020. Coastline shown in heavy black, and study region for (d) shown by white square in (c). Blue and green dots over water and land, respectively, indicate locations of model wind profiles in Fig. 12.

The flow was nearly parallel to the coast, with the higher z_0 associated with the land areas onshore to the right of the wind vector. This produced substantial negative vertical vorticity (and circulation) along the coast, as 10-m AGL windspeeds over the water just 5 km offshore (blue dot, Fig. 11b) were >36 kt (18 m s^{-1}), while winds were only 22 kt (11 m s^{-1}) 5 km onshore (green dot, Fig. 11b). Typical vorticity values resolved by the HRRR model along the coast were near -1.5×10^{-3} s^{-1}. The overland 0–500-m AGL vector (bulk) wind difference was 17.6 m s^{-1} while over the water, just 10 km away, it was 11.5 m s^{-1}. The 0–1-km bulk wind difference was 21.8 m s^{-1} over the land, and 17.7 m s^{-1}, over the water. Also, only 10 km inland, southeasterly winds over St. Andrew's Bay were near 13 m s^{-1}, while winds over land just to the south were 11 m s^{-1}, producing positive vorticity.

b. Mobile Bay, AL, and Pensacola Bay, FL

Several hours later, at 0100 UTC 17 September 2020, the center of what was then Tropical Storm Sally was over south-central Alabama (Fig. 11c). The winds over Mobile Bay were generally below tropical storm force, but fairly uniformly north-northwesterly. Winds over Pensacola Bay, 75–100 km east of Mobile Bay, were generally from the west-northwest.

Note the rapid adjustment in the HRRR winds at 10 m AGL from land over southwest Alabama to lower-z_0 water over Mobile Bay and the Gulf of Mexico (Fig. 11d). Divergence values near 5×10^{-4} s^{-1} occurred over northern Mobile Bay. Once the winds fully adjusted over the open waters of the bay, 10-m AGL windspeeds were >20 kt (10 m s^{-1}), while winds over adjacent land were only 12 kt (6 m s^{-1}). This produced positive vorticity on the eastern shore of Mobile Bay of ~10^{-3}s^{-1}. Negative vorticity was produced on the western shore. Similar acceleration of winds, and the production of vertical vorticity, were simulated over Pensacola Bay.

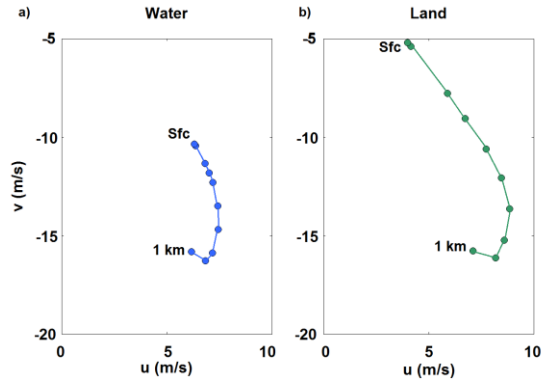

Figure 12: Hodographs of HRRR model surface to 1-km winds (m s^{-1}) near Mobile Bay at 0100 UTC 17 September 2020, a) over water (blue) and b) over land (green). The geographic locations of each model wind profile are shown in Fig. 11d.

As discussed in sections 1 and 3c, vertical wind shear is also expected to be larger over areas with higher values of z_0. HRRR windspeed profiles were retrieved over the water and over the land near Mobile Bay, at points 20 km apart (see Fig. 11d, 12), and are consistent with the notion of greater shear over lower roughness. Winds were from 323° at 10.5 m s^{-1} over water, but from 310° at 5.4 m s^{-1} over land, so there was 13° of backing over land, and speeds were 5.1 m s^{-1} lower over land than over water. The speeds over land were slower up through about 800 m AGL. The 0–500 m bulk wind difference over the land was 9.5 m s^{-1}, while over the water it was only 4.4 m s^{-1}. The 0–1-km bulk wind difference shear was 10.8 m s^{-1} over the land, and only half that value, 5.4 m s^{-1}, over the water.

c. Lake Wheeler, AL

Here, we examine the flow acceleration over a relatively small inland body of water (main part of lake 1.5–3 km wide, about 25 km long, Fig. 13a) surrounded by a combination of pastureland, cropland, and some developed urban land, using the HRRR. Thirteen study days from 2020 were chosen using wind observations from nearby station KMSL (section 2). A total of 8 days with up-lake winds (from the west-northwest) and 5 days with down-lake winds (from the east-southeast) were identified. Seven were during the cold season (when water is warmer than land) and 6 were during the warm season.

Figure 13b shows stronger HRRR 10-m AGL winds over the lake in each case. The mean difference between the spatially averaged windspeed over the lake and over the land 8–12 km either side of the lake was 1.7 m s^{-1}, and the ratio of lake/land windspeeds averaged 1.42. In all 13 cases, positive (negative) vorticity was produced on the side of the lake that was to the left (right) of the wind vector.

An example case is shown (Fig. 13c) from 6 May 2020, at 1200 UTC. During this warm-season up-lake wind event, a cold front had passed through the region 12–18 h prior. Overlake windspeeds at 10 m AGL peaked at 7.6 m s^{-1} (average 7.2 m s^{-1}), but on the land around the lake, winds were generally 4–6 m s^{-1} (average 5.4 m s^{-1}). This generated positive (negative) vorticity on the north (south) side of the lake.

HRRR wind profiles were analyzed along cross section AB (Fig. 13c), to determine how the model depicted the depth of horizontal and vertical wind shear. Wind profiles were retrieved every 3 km in the horizontal, the grid spacing of the HRRR. The cross section of windspeed is shown in Fig. 14. In the HRRR, the primary wind perturbation over the lake is

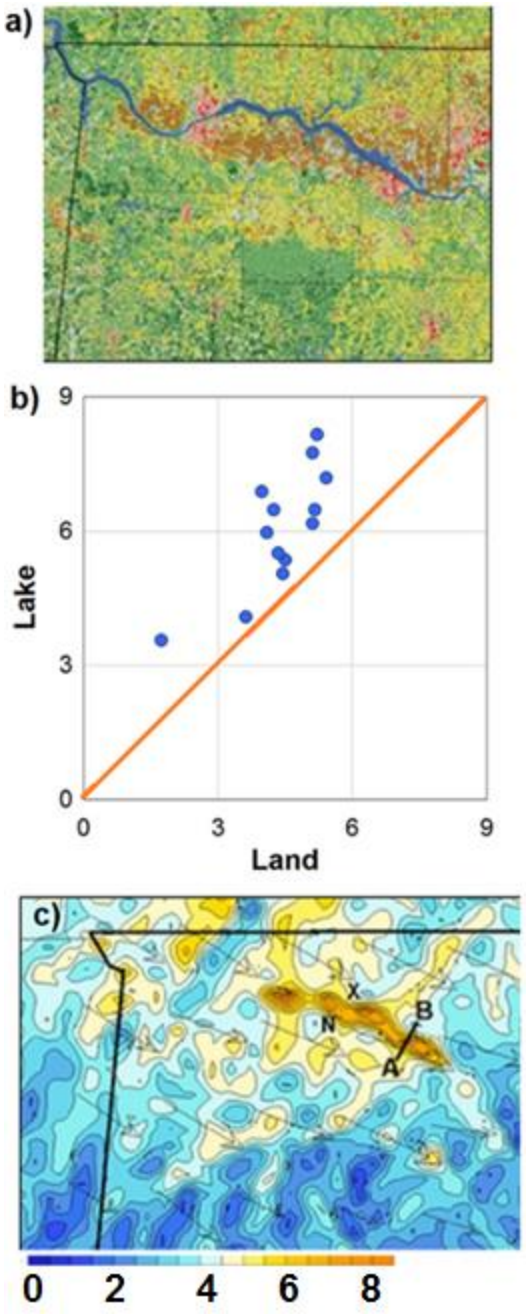

Figure 13: a) Lake Wheeler area map with NLCD land-cover types (MRLC 2021). b) Scatterplot of 2020 case studies, showing average 10 m AGL windspeed over land around the lake vs. over the lake (m s^{-1}). c) HRRR 10-m wind vectors and windspeed contours (every 0.5 m s^{-1}) in the area of Lake Wheeler, AL, at 1200 UTC 6 May 2020. AB line segment refers to cross section in Fig. 14. Alabama state line in heavy black.

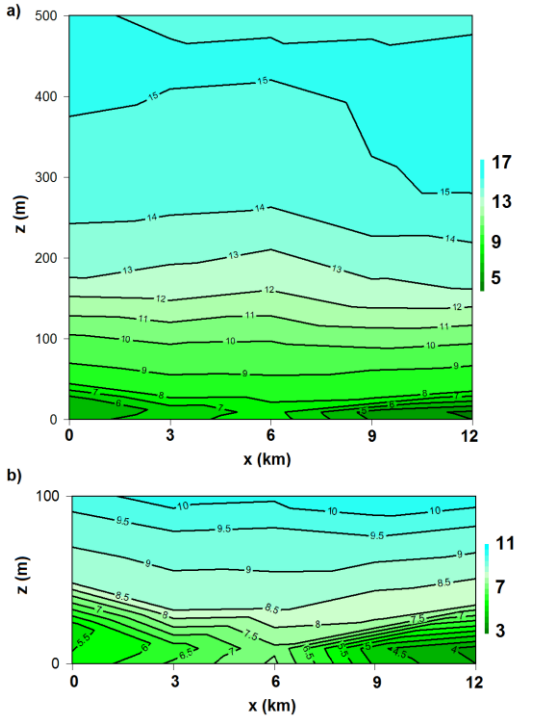

Figure 14: a) Cross section of HRRR model windspeeds (m s^{-1}) across line AB in Fig. 13a. b) As in (a), but zoomed to the lowest 100 m AGL.

below 50 m AGL, but some perturbation is notable up to 400 m AGL. This is different than Fig. 6 (data during an unstable summer afternoon), when vorticity was measured above 1 km AGL. This implies that stability may confine the effects of differential friction to lower levels, while instability allows the effects to reach higher levels (e.g., Stull 1988). The vertical wind speed shear is much larger over the land than over the water (Fig. 14).

d. Northeastern Arkansas

Hua and Chavas (2019) found that tornadoes in Arkansas were less likely in areas with higher terrain roughness, such as west-central and northwestern Arkansas (their Fig. 1). However, there is also a large *gradient* in surface roughness length (z_0), specifically in northeastern Arkansas, between the cropland in the Mississippi River Delta (z_0 = 0.06 m) and the regions of pasture and deciduous forest (z_0 = 0.06 to 0.65 m) over north-central Arkansas (Fig. 15a). The gradient in z_0 is incorporated into the HRRR model (Fig. 15b).

Eighteen study days with 10-m AGL winds >5 m s^{-1} winds over northeast Arkansas (section 2) were chosen from nine different months of the year, and for different flow directions (parallel to the z_0 gradient, normal to the z_0 gradient, and angles in between). Hours meeting these criteria then were chosen randomly, to eliminate any bias due to different geostrophic winds. Then, HRRR 10 m AGL winds from two locations 45 km apart, 36°N, 91°W (over cropland, blue dot in Fig. 15b) and 36°N, 91.5°W (over forest, white dot in Fig. 15b), were compared for these days. The results show that wind over the smoother cropland consistently blows faster than the winds over the rougher forest, similar to section 5c. The mean difference between the HRRR windspeed over the cropland and the forest was 1.8 m s^{-1}, and the ratio of cropland/forest windspeeds averaged 1.23.

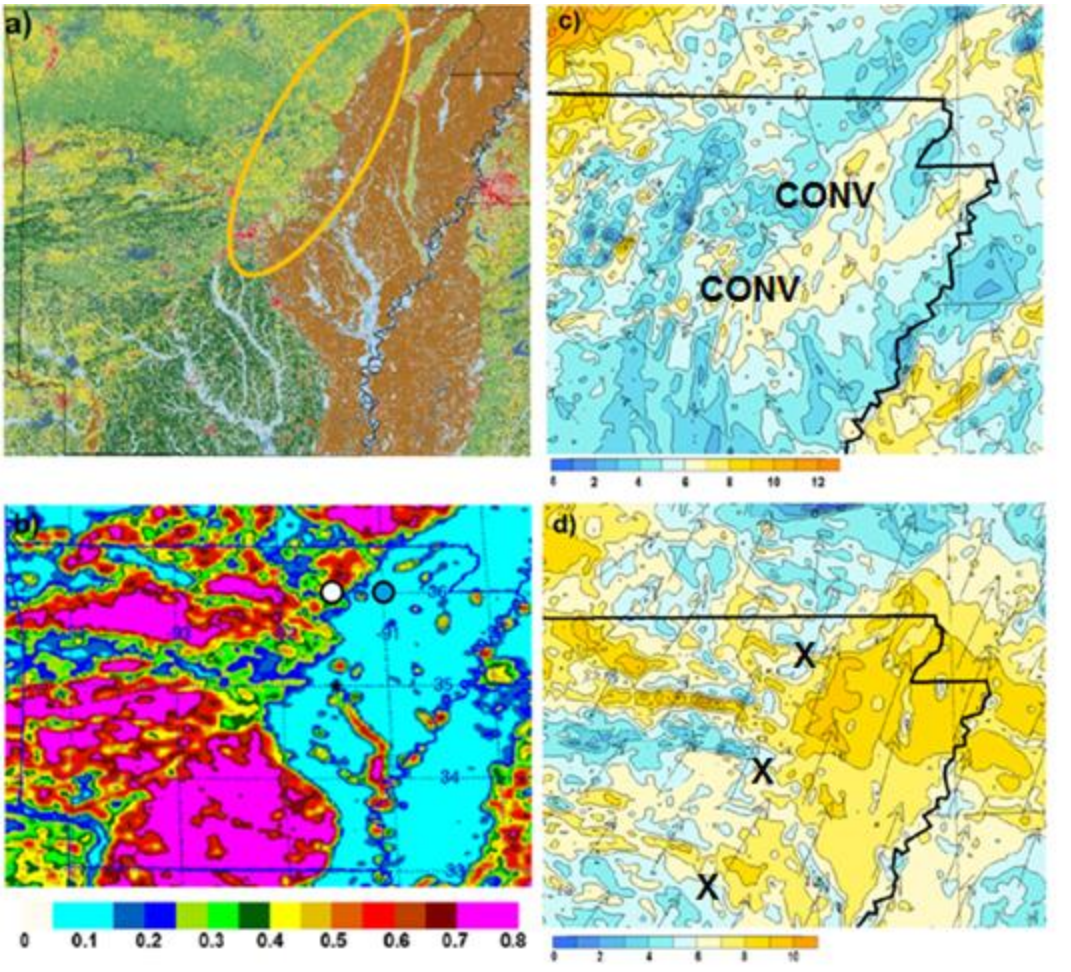

Figure 15: a) Arkansas map with NLCD land-cover types (MRLC 2021); b) HRRR roughness length (m) over Arkansas. The white and blue dots along 36° north latitude are referred to in the text. c) HRRR 10-m wind vectors and windspeed contours (m s^{-1}) over northern and eastern Arkansas at 2100 UTC 10 January 2020 and d) HRRR model 10-m wind vectors and speed contours (m s^{-1}) over northern and eastern Arkansas at 1800 UTC 12 March 2020. Arkansas state line shown in heavy black. As previously, the "X"s indicate positive vorticity.

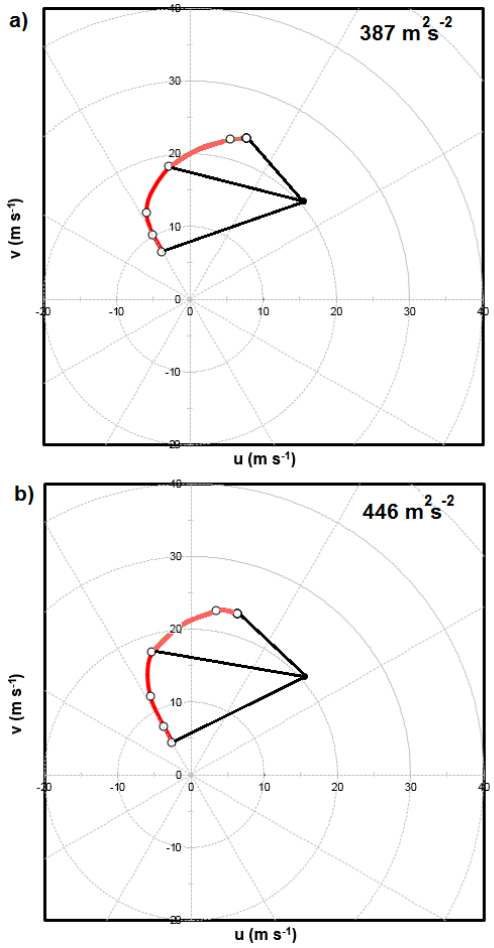

Figure 16: HRRR model 0–1-km hodographs at 2100 UTC 10 January 2020 at a) the location of the blue dot in Fig. 15b (cropland), and b) the location of the white dot in Fig. 15b (forest).

In addition, to examine differences in vertical wind shear over different z_0, the magnitudes of the 0–500-m AGL and 0–1-km bulk wind difference were calculated from HRRR model soundings at the two points shown in Fig. 15b. Larger shear would be expected over the rougher terrain (sections 3c, 4b), and this was indeed the case. The average 0–500-m AGL bulk wind difference was 1.1 m s^{-1} larger over the rougher terrain than over the smooth terrain; the average 0–1-km bulk wind difference was 1.7 m s^{-1} larger over rough terrain. One of these 18 cases, 10 January 2020, was a severe-weather day over Arkansas, with eleven tornadoes (NWS 2020a). The storm motion was determined, as in other cases herein, to be from 229° at 20 m s^{-1}. Hodographs of the HRRR 0–1-km wind profiles, along with storm-relative wind vectors, from 2100 UTC 10 January 2020 are plotted in Fig. 16. Over the smoother cropland (Fig. 16a), the simulated 0–1-km SRH was 387 m^2 s^{-2}; over the rougher forest and pastureland (Fig. 16b) the 0–1-km SRH was 446 m^2 s^{-2}, about 15% higher.

Two cases were selected to show two different processes that can occur along the sharp gradient in z_0 in northeast Arkansas. One is 10–11 January 2020 (Fig. 15c), when the HRRR model surface flow at 2100 UTC was from the southeast. Over the cropland of extreme northeastern Arkansas, windspeeds were mainly 5–8 m s^{-1}, while over the mixed forest and pastureland of north central Arkansas, windspeeds were generally 3–6 m s^{-1}. This situation created convergence along the southwest-to-northeast gradient in z_0. Another severe-weather event over Arkansas was 12 March 2020 (NWS 2020b). In this case, however, low-level winds were out of the south-southwest (Fig. 15d). The HRRR surface windspeeds at 1800 UTC 12 March 2020 average about 8 m s^{-1} over the cropland area, and about 6 m s^{-1} over the undisturbed areas over the forest. This flow regime produced positive vorticity (indicated, as before, by X) and circulation along the sharp gradient in z_0 over northeast Arkansas.

Likely, not all of the heterogeneity in windspeed, direction, or shear, shown in Figs. 11 through 16, is due only to differences in z_0. Also, even though the horizontal grid spacing in the HRRR model is only 3 km, differences in windspeed, direction, and shear, even over features like Lake Wheeler (Fig. 13) that are only about 5 km wide, are apparent. Validation of convection-allowing model wind profiles at higher resolutions is needed, specifically in regions with heterogeneous surface roughness.

6. Discussion and conclusions

Conceptually, airflow over a region with a gradient in roughness length (z_0) can cause quasi-ambient vertical vorticity and/or horizontal divergence. This is shown schematically and numerically herein. In addition, given a logarithmic wind profile, near-surface wind-speeds are lower, and wind shear is higher, over areas with higher z_0. Once the force balance for wind in the presence of friction is analyzed, winds slowing to subgeostrophic speeds due to friction clearly result in backing of the wind direction. Since the effect of friction decreases with height, so does the backing, resulting in

veering with height over rough surfaces, and increased SRH relative to areas with similar geostrophic wind profiles but lower z_0. Even though there are several assumptions made in the derivation of the Ekman spiral wind profile, it contains helicity due purely to surface friction (e.g., Markowski and Richardson 2010, pp. 81–82).

Single- and dual-Doppler radar analyses and HRRR numerical simulations also indicate that differential friction may produce regions of quasi-ambient vertical vorticity ~10^{-3} to 10^{-2} s^{-1}. Determination of the exact vorticity associated with airflow over differential z_0 is difficult due to limitations in the horizontal scale of observations, and the scale and parameterization of horizontal diffusion in numerical simulations, whether in high-resolution (500-m horizontal grid) simple models like the one shown in Fig. 4, or in the HRRR (3-km horizontal grid). However, substantial circulation is apparent in HRRR simulations in tropical cyclone winds parallel to the Gulf Coast. Convergence associated with a convective storm could access such circulation and, through convergence, produce large values of vertical vorticity. Such vorticity and circulation, positive or negative, may be ingested into the updraft of a storm, either intensifying or weakening any incipient mesocyclone. Airflow over differential z_0 may also produce horizontal convergence. Such convergence may not only impact convective initiation, but also amplify vertical vorticity through stretching in a preexisting convective updraft.

Observations during VORTEX-SE 2020 and 2021 IOPs also show that in nearby areas (within 65 km), with similar profiles of geostrophic wind, locations of higher surface roughness exhibit stronger vertical wind shear and storm-relative helicity. HRRR simulations in areas with z_0 gradients also show stronger vertical wind shear and SRH over rough areas vs. smoother areas. Recent findings (e.g., Coffer and Parker 2018), combined with the observed and simulated impact of z_0 on SRH, indicate that z_0 should be considered as a potential factor in tornadogenesis.

Several authors have examined the relationship between tornadoes and surface roughness directly (e.g., Dessens 1972; Leslie 1977; Lewellen et al. 2000; Bluestein 2000; Dunn and Vasiloff 2001; Kellner and Niyogi 2014; Jagger et al. 2015; Roberts et al. 2016; Dawson et al. 2019). Schenkman et al. (2014) found that, in numerical simulations of the 8 May 2003 Oklahoma City supercell, the tornado was longer-lived with friction than without it. Markowski et al. (2019) show that even the BL Monin-Obukhov similarity theory used in many numerical models underestimates vertical wind shear in storm outflow near the surface, where friction is most prevalent. Parker (2014) and Coffer et al. (2017) suggest that near-surface SRH and streamwise vorticity are the best differentiators between tornadic and nontornadic supercells. Both of these parameters are affected by changes in z_0.

Given the large heterogeneity in land cover in the central and eastern United States, there are numerous areas, even within single National Weather Service office county warning areas, where differential surface roughness may produce locations that are more or less favorable for tornadogenesis than others only a few km away. Markert et al. (2019) found that there are statistically significant patterns in tornadogenesis climatology related to gradients in z_0. In light of the many recent studies that indicate near-surface vorticity, convergence, and vertical wind shear, similar to that associated with friction, may play a role in tornadogenesis and tornado intensity, it is relevant to examine these processes, and the areas where they occur, in more depth.

In the formal version of ongoing research (e.g., Coleman and Weigel 2016), we plan to examine several areas across the United States where gradients in z_0, given flow from certain directions, produces regions of quasi-ambient vertical vorticity and divergence. Climatological maxima (minima) in tornadogenesis are often consistent with areas of positive (negative) vorticity, convergence (divergence), and regions of roughness-amplified (lessened) SRH. Comparisons of roughness-induced SRH differences clearly would be more meaningful for locations much less than 65 km apart. We plan to conduct a more systematic study comparing wind profiles (derived using 915-MHz wind profilers, Doppler wind lidar, and sodar), from KHSV and UAH. Examples of tornadogenesis and tornadolysis, when a mesocyclone was over a favorable (unfavorable) region based on z_0 effects, are also being examined.

ACKNOWLEDGMENTS

The authors wish to thank Amanda Markert for her detailed research and sharing of data on the subject of this paper. We also thank Eric Lenning of NWS Chicago, Roger Edwards of the Storm Prediction Center, and Jason Simpson of WHNT-TV in Huntsville, AL, for thoughtful discussions on the material. Finally, we thank the editor and the reviewers, whose contributions made the paper much better, as they always do. This research was funded by NOAA via NGI contract 191001.363513.04G.

REFERENCES

Air Resources Laboratory (ARL), cited 2021: Archived meteorology. [Available online at https://www.ready.noaa.gov/READYamet.php.]

AMS, 2019: *Glossary of Meteorology*, "aerodynamic roughness length." [Available online at https://glossary.ametsoc.org/wiki/Aerodynamic_roughness_length.]

Anderson-Frey, A. K., and H. E. Brooks, 2019: Tornado fatalities: An environmental perspective. *Wea. Forecasting*, **34**, 1999–2015.

Arya, S. P., 1988: *Introduction to Micrometeorology*, Academic Press, 307 pp.

Asefi-Najafabady S., K. Knupp, J. R. Mecikalski,and R. M. Welch, 2012: Radar observations of mesoscale circulations induced by a small lake under varying synoptic-scale flows. *J. Geophys. Res. Atmos.*, **117**, D01106.

——, K. Knupp, J. R. Mecikalski, R. M. Welch, and D. Phillips, 2010: Ground-based measurements and dual-Doppler analysis of 3-D wind fields and atmospheric circulations induced by a meso-γ-scale inland lake. *J. Geophys. Res. Atmos.*, **115**, D23117.

Ashley, W. S., 2007: Spatial and temporal analysis of tornado fatalities in the United States: 1880–2005. *Wea. Forecasting*, **22**, 1214–1228.

Bluestein, H. B., 1992: *Synoptic-Dynamic Meteorology in Midlatitudes.* Vol. I. Oxford University Press, 431 pp.

——, 2000: A tornadic supercell over elevated, complex terrain: The Divide, Colorado storm of 12 July 1996. *Mon. Wea. Rev.*, **128**, 795–809.

Bothwell, P. D., J. A. Hart, and R. L. Thompson, 2002: An integrated three-dimensional objective analysis scheme in use at the Storm Prediction Center. Preprints, *21st Conf. on Severe Local Storms*, San Antonio, TX, Amer. Meteor. Soc., JP3.1.

Bou-Zeid, E., W. Anderson, G. G. Katul, and L. Mahrt, 2020: The persistent challenge of surface heterogeneity in boundary-layer meteorology: A review. *Bound.-Layer Meteor.*, **177**, 227–245.

Carlson, T. N., 1991*: Mid-latitude Weather Systems.* Harper-Collins Academic, 507 pp.

Coffer, B. E., M. D. Parker, R. L. Thompson, B. T. Smith, and R. E. Jewell, 2019: Using near-ground storm relative helicity in supercell tornado forecasting. *Wea. Forecasting*, **34**, 1417–1435.

——, and M. D. Parker, 2018: Is there a ''tipping point'' between simulated nontornadic and tornadic supercells in VORTEX2 environments? *Mon..Wea. Rev.*, **146**, 2667–2693.

——, M. D. Parker, J. M. Dahl, L. J. Wicker, and A. J. Clark, 2017: Volatility of tornadogenesis: An ensemble of simulated nontornadic and tornadic supercells in VORTEX2 environments. *Mon..Wea. Rev.*, **145**, 4605–4625.

Coleman, T. A., and A. M. Weigel, 2016: The effects of differential friction on PBL kinematics and possible influences on mesocyclones and tornadoes. Proc., *28th Conf. on Severe Local Storms*, Portland, OR, Amer. Meteor. Soc., 3.4.

Coniglio, M. C., 2012: Verification of RUC 0–1-h forecasts and SPC mesoscale analyses using VORTEX2 soundings. *Wea. Forecasting*, **27**, 667–683.

Davies-Jones, R., 1984: Streamwise vorticity: The origin of updraft rotation in thunderstorms. *J. Atmos. Sci.*, **41**, 2991–3006.

Dawson, D. T., B. Roberts, and M. Xue, 2019: A method to control the environmental wind profile in idealized simulations of deep convection with surface friction. *Mon. Wea. Rev.*, **147**, 3935–3954.

Dessens, J., 1972: Influence of ground roughness on tornadoes: A laboratory simulation. *J. Appl. Meteor.*, **11**, 72–75.

Dunn, L. B., and S. V. Vasiloff, 2001: Tornadogenesis and operational considerations of the 11 August 1999 Salt Lake City tornado as seen from two different Doppler radars. *Wea. Forecasting*, **16**, 377–398.

Garratt, J. R., 1992: *The Atmospheric Boundary Layer*. Cambridge University Press, 316 pp.

Geernaert, G. L., 2003: Surface layer. *Encyclopedia of Atmospheric Sciences*, J. Holton, J. Pyle, and J. Curry, Eds. Los Alamos National Laboratory, 305–311.

Gentry, R. C., 1983: Genesis of tornadoes associated with hurricanes. *Mon. Wea. Rev.*, **111**, 1793–1805.

Grimmond, C. S. B., and T. R. Oke, 1999: Aerodynamic properties of urban areas derived from analysis of surface form. *J. Appl. Meteor. Climatol.*, **38**, 1262–1292.

Hartley, S., R. Pace III, J. B. Johnston, M. Swann, C. O'Neil, L. Handley, and L. Smith, 2000: A GAP analysis of Louisiana: Final report and data. U.S. Department of the Interior, U.S. Geological Survey, Lafayette, LA, 588 pp.

Holton, J.R., 1992: *An Introduction to Dynamic Meteorology.* 3rd Ed. Academic Press, 511 pp.

Hua, Z., and D. R. Chavas, 2019: The empirical dependence of tornadogenesis on elevation roughness: Historical record analysis using Bayes's Law in Arkansas. *J. Appl. Meteor. Climatol.*, **58**, 401–411.

Jagger, T. H., J. B. Elsner, and H. M. Widen, 2015: A statistical model for regional tornado climate studies. *PLOS ONE*, **10**, e0131876.

Kellner, O., and D. Nikyogi, 2014: Land surface heterogeneity signature in tornado climatology? An illustrative analysis over Indiana, 1950–2012. *Earth Interactions*, **18**, 1–32.

Kristovich, D. A., L. Bard, L. Stoecker, and B. Geerts, 2018: Influence of Lake Erie on a Lake Ontario lake-effect snowstorm. *J. Appl. Meteor. Climatol.*, **57**, 2019–2033.

Lee, T. R., M. Buban, D. D. Turner, T. P. Meyers, and C. B. Baker, 2019: Evaluation of the High-Resolution Rapid Refresh (HRRR) model using near-surface meteorological and flux observations from northern Alabama. *Wea. Forecasting*, **34**, 635–663.

Leslie, F. W., 1977: Surface roughness effects on suction vortex formation: A laboratory simulation. *J. Atmos. Sci.*, **34**, 1022–1027.

Lewellen, D. C., W. S. Lewellen, and J. Xia, 2000: The influence of a local swirl ratio on tornado intensification near the surface. *J. Atmos. Sci.*, **57**, 527–544.

Liang, X., 2007: An integrating velocity-azimuth process single-Doppler radar wind retrieval method. *J. Atmos. Oceanic Technol.*, **24**, 658–665.

Markert, A., R. Griffin, K. Knupp, A. Molthan, and T. Coleman, 2019: A spatial pattern analysis of land surface roughness heterogeneity and its relationship to the initiation of weak tornadoes. *Earth Interactions*, **23**, 1–28.

Markowski, P. M., and Y. Richardson, 2010: *Mesoscale Meteorology in Midlatitutes.* Wiley & Sons, 407 pp.

——, and ——, 2007: Observations of vertical wind shear heterogeneity in convective boundary layers. *Mon. Wea. Rev.*, **135**, 843–861.

——, N. T. Lis, D. D. Turner, T. R. Lee, and M. S. Buban, 2019: Observations of near-surface vertical wind profiles and vertical momentum fluxes from VORTEX-SE 2017: Comparisons to Monin–Obukhov similarity theory. *Mon. Wea. Rev.*, **147**, 3811–3824.

Minder, J. R., W. M. Bartolini, C. Spence, N. R. Hedstrom, P. D. Blanken, and J. D. Lenters, 2020: Characterizing and constraining uncertainty associated with surface and boundary layer turbulent fluxes in simulations of lake-effect snowfall. *Wea. Forecasting*, **35**, 467–488.

Multi-Resolution Land Characteristics Consortium, cited 2021: 2016 CONUS Land Cover. [Available online at https://www.mrlc.gov/viewer/.]

National Hurricane Center, 2020a: Hurricane Sally advisory archive. [Available online at https://www.nhc.noaa.gov/archive/2020/al19/al192020.update.09160956.shtml.]

National Hurricane Center, 2020b: Sally graphics archive: Initial wind field and watch/warning graphic. [Available online at https://www.nhc.noaa.gov/archive/2020/SALLY_graphics.php

NOAA, cited 2021: The High-Resolution Rapid Refresh (HRRR). [Available online at https://rapidrefresh.noaa.gov/hrrr/.]

National Weather Service, 2020a: Severe storms/heavy rain on January 10–11, 2020. [Available online at https://www.weather.gov/lzk/svr0120.htm.]

National Weather Service, 2020b: Severe weather and areas of heavy rain on March 11–15, 2020. [Available online at https://www.weather.gov/lzk/svr0320.htm.]

Parker, M. D., 2014: Composite VORTEX2 supercell environments from near-storm soundings. *Mon. Wea. Rev.*, **142**, 508–529.

Persson, P., and T. Andersson, 1987: A real-time system for automatic single-Doppler wind field analysis. Proc., *Symp. on Mesoscale Analysis and Forecasting*, Vancouver, BC, Canada, ESA Publication SP-282, 61–66.

Petersen, W. A., and coauthors, 2005: The UAH-NSSTC/WHNT ARMOR C-band dual-polarimetric radar: A unique collaboration in research, education and technology transfer. Preprints, *32nd Conf. on Radar Meteorology*, Albuquerque, NM, Amer. Meteor. Soc., 12R4.

Rauber, R. M., J. Walsh, and D. Charlevoix, 2019: *Severe and Hazardous Weather: An Introduction to High Impact Meteorology*. 5th Ed. Kendall Hunt, 277 pp.

Reames, L. J., and D. J. Stensrud, 2018: Influence of a Great Plains urban environment on a simulated supercell. *Mon. Wea. Rev.*, **146**, 1437–1462.

Roberts, B., M. Xue, A. D. Schenkman, and D. T. Dawson, 2016: The role of surface drag in tornadogenesis within an idealized supercell simulation. *J. Atmos. Sci.*, **73**, 3371–3395.

Schenkman, A. D., M. Xue, and M. Hu, 2014: Tornadogenesis in a high-resolution simulation of the 8 May 2003 Oklahoma City supercell. *J. Atmos. Sci.*, **71**, 130–154.

Storm Prediction Center, cited 2021: Archive national sector, SPC hourly mesoscale analysis. [Available online at https://www.spc.noaa.gov/exper/ma_archive/.]

Stull, R. B., 1988: *An Introduction to Boundary Layer Meteorology*. Kluwer Academic Publishers, 684 pp.

Tao, Z., 1992: The VAP method to retrieve the wind vector field based on single-Doppler velocity field. *Acta Meteor. Sin.*, **50**, 81–90.

Tennekes, H., 1973: The logarithmic wind profile. *J. Atmos. Sci.*, **30**, 234–238.

University of Illinois Urbana-Champaign, cited 2021: The Weather World 2010 Project. [Available online at http://ww2010.atmos.uiuc.edu/(Gh)/guides/mtr/fw/fric.rxml.]

Welsh, D., B. Geerts, X. Jing, P. T. Bergmaier, J R. Minder, W. J. Steenburgh, and L. S. Campbell, 2016: Understanding heavy lake-effect snowfall: The vertical structure of radar reflectivity in a deep snowband over and downwind of Lake Ontario. *Mon. Wea. Rev.*, **144**, 4221–4244.

REVIEWER COMMENTS

[Authors' responses in *blue italics.*]

REVIEWER A (Paul M. Markowski):

Initial Review:

Recommendation: Accept with major revisions.

Substantive Comments: Re: Logarithmic wind profile: Lots of assumptions here, and in fact, one of them is horizontal *homogeneity*. Need to state them, and also explain the paradox of how you're implicitly assuming horizontal homogeneity in invoking a log profile, but then using this profile to demonstrate how horizontal heterogeneity in z_0 leads to heterogeneity in mean wind. Also, the log profile is for the mean wind, not instantaneous wind.

The horizontal homogeneity you refer to for the log wind profile is over a very small area (~100 m or less), while our gradients in roughness length for this paper (and log wind profiles) are over [multiple] km. There is no paradox here. You are correct that it is for the mean wind, and we add that, but the reader gets the point, and there is no reason to complicate this simple principle.

Surprised there's no mention of the analytical expression for the mean wind shear assuming a log mean wind profile.

We added the expression for mean wind shear in a neutral surface layer (SL).

I don't understand what it means to have a "linear transition scheme." If each grid point has a certain z_0 associated with it, then the variation from grid point to grid point is obviously linear (two points define a line). But nothing happens in between grid points anyway.

Changed wording. We are talking about multiple grid points, so we added the word "spatial". It is not a binomial or exponential transition here nor in the HRRR, but a linear one.

Numerical diffusion or turbulent diffusion? If an odd-ordered advection scheme is used, then explicit (parameterized) numerical diffusion is typically not applied. And w.r.t. turbulent diffusion, in high-res simulations (I assume the authors are referring to LES), the energy-containing eddies are well-resolved (this is a fundamental requirement of LES). Thus, there's little parameterized turbulent diffusion, at least above the first grid level.

We are referring to turbulent diffusion, and added wording to indicate. We are referring to operational models like HRRR and NAM, so removed "high-resolution", as we can see how that would indicate to many readers LES, CM1, etc.

Re: conservation of absolute circulation in Kelvin's theorem: This is only true in the inviscid, barotropic limit. But isn't there friction here? C would not be conserved in that case.

You are correct. As one of the other reviewers noted, it only applies to a "useful approximation" in the large convergence in a supercell storm. We restated this section.

Re: SL winds nearly geostrophic over smooth surfaces: Assuming the flow is straight? If this is an assumption, please say so. If it's not assumed, then doesn't the centrifugal force need to be considered as well? (Fig. 5 implies straight flow, but there's no mention of this assumption in the text.)

You are correct, and we thought about bringing gradient wind/centrifugal force in but decided it would unnecessarily complicate things. The assumption of straight flow was added, though, and we are glad you noted that!

Re: Lake Wheeler vertical-vorticity cross section: It's not obvious to me that the ζ anomalies here are the result of horizontal gradients in z_0. Most of the positive ζ is over the lake, not where the gradient in z_0 would be a maximum (i.e., along the shoreline). And the dominant perturbation winds are offshore, not downstream along the lake axis; this suggests that the lake-breeze effect is dominant. And if there are counter-rotating (horizontal) lake-breeze circulations, then there's a horizontal gradient of *w* and tilting of ambient horizontal vorticity; in fact, such tilting of horizontal vorticity would be consistent with the observed ζ pattern. Bottom line, how is it known that these ζ perturbations are the result of z_0 gradients and not something else, such as tilting? Moreover, how are winds down to z = 0 determined in the vertical cross section? That would require extrapolation.

Asefi et al. (2010) Fig. 13a shows that, especially in the northern half of the lake, the perturbation wind is down the lake, not in the thermally direct baroclinic circulation, and in no part of the lake is the thermally direct circulation clearly the dominant perturbation. Examination of Asefi et al. (2010), Figs. 11 and 12, show that the perturbation vertical velocity over and near the lake is generally negative. Coming from no lake, any tilting of the baroclinically-generated horizontal vorticity would actually produce the opposite effect…with positive vertical vorticity on the right side of the wind vector (south) and negative vertical vorticity on the left side (north). This strengthens our position that differential friction must be producing these vertical vorticity perturbations.

Regarding the data down to near z =0, there must have been some extrapolation by Asefi et al. (2010). However, not much, since both the MAX and ARMOR radars used to produce these analyses were in very close proximity to the lake.

The hodographs have differences, but why are we assuming the differences are the result of differences in z_0?

Added "most of this difference is due to the slowed and backed surface winds at UAH." As we note in the paper, average surface wind at CTD was 183°/4, while at UAH it was 169°/3.4. It was backed and slowed at UAH. RAP/SPC mesoanalysis shows that SRH at these locations should be the same.

Re: No boundaries between CTD and UAH at 1700 UTC: [T]here is typically SRH variability in the absence of mesoscale boundaries, and in fact the SPC mesoanalysis are proof of this (i.e., the SPC mesoanalysis don't show flat fields away from mesoscale boundaries). See also Markowski et al. (1998, MWR, "Variability of SRH during VORTEX") and Markowski and Richardson (2007, MWR, "Observations of vertical wind shear heterogeneity in convective boundary layers").

Sure, there are other causes of heterogeneity in SRH, as you discuss in your papers. But, if I understand correctly, these would be transient. There is a theoretical reason for SRH to be consistently higher at UAH than CTD, namely z_0, and Fig. 10 shows that there is a consistent, predictable difference in SRH between UAH and CTD. In "homogeneous" environments, your paper shows variability in 0–1-km SRH of about 15 $m^2 s^{-2}$, ours shows much larger differences. Figure 8 also shows the wind speed at KHSV (lower z_0) was, on average, 1–2.5 m s^{-1} higher than at UAH (higher z_0) over 2688 15-min intervals. However, we refer to Markowski and Richardson (2007) as a caveat in 4b.

Re: UAH winds backed and slowed due to higher z_0: There is no way to know this given that it not known whether the HPGF is the same at these two locations.

Average surface winds were 181°/5.5 at CTD, 154°/3.8 at UAH. It is extremely unlikely, given the homogeneous environment implied by SPC mesoanalysis (no boundaries, etc.) that the horizontal pressure gradient force was 29% smaller and 27 degrees backed at UAH vs. CTD. But, we changed the wording to say "it is likely" on z_0 causing difference.

Any differences in the averaging used by these two different [UAH, CTD] instruments? Why are the winds at UAH so much faster just above the surface than at CTD? Seems to argue against z_0 being the source of SRH variability. In fact, the biggest hodograph differences appear to be in the upper BL, not at the surface.

One of the authors is producing a thesis on the consistency and accuracy of wind measurements across these instruments, and has found that the errors are generally <1 m s^{-1}.

The notion of "simultaneous rawinsonde pairs" is problematic. See Markowski and Richardson (2007).

See [UAH vs. CTD comments above]. They are indeed simultaneous, and we are showing a pattern of higher SRH at one point vs. another that is consistent in time and across IOPs.

Re: Hurricane Sally effects on St. Andrews Bay flow: 1) This isn't much circulation about a circuit this large; 2) the circulation is negative, right?; 3) why do supercells in the rainbands of TCs not weaken when ingesting this anticyclonic vorticity if this vorticity is so important?

Coleman research shows that supercells in tropical cyclones often do weaken as they approach the coast when alongshore flow is producing negative vorticity and circulation.

Re: Fig. 15 caption: [H]ow is convergence deduced from one wind component? Is it being assumed that $\partial V/\partial n = 0$ everywhere? This is not a great assumption.

If one examines panel (b), it is obvious that convergence would occur due to z_0 increase with SE winds. In addition, one can examine the vectors in panel (c) and readily determine that convergence is occurring. Your point is well taken, but dV/dn could be positive or negative due to effects outside of friction, enhancing or weakening the convergence. We are focusing on z_0-induced convergence.

Circulation depends on the areas being considered, and a particularly large area was chosen here. One could double these values simply by doubling the area, but the physics wouldn't change. Bottom line: these values are fairly arbitrary, so it doesn't mean much to cite them here.

We removed the magnitudes of circulation…you are right that it depends on the size of the area.

I'm surprised there's no reference to the Ekman spiral anywhere in the paper, or a comparison of the Ekman spiral's helicity as a function of z_0. The Ekman spiral has a few issues [e.g., it is dynamically unstable (inflection-point instability), assumes no horizontal T gradient, no vertical gradient of eddy viscosity], but it would at least provide a theoretical framework for what the authors are trying to do w.r.t. the effect of z_0 on vertical wind profiles and SRH.

Added mention of Ekman spiral and referenced Markowski and Richardson (2010).

[Minor comments omitted…]

Second Review:

Recommendation: Accept with major revisions.

Dr. Markowski: Thanks again for your thorough review of our paper and your thinking outside the box on it. We answer your comments individually below, and made the associated changes to the manuscript.

Substantive Comments: I don't understand Fig. 2 and its caption. I guess I'm hung up on "top" and "bottom." I cannot figure out what top and bottom refer to. I also cannot figure out what the westward and eastward pointing vectors in (a) and (b) are. They are labeled as convergence and divergence, but convergence and divergence aren't vectors. These vectors don't appear to be velocity vectors either.

I see what you are saying here. Other reviewers and one of my co-authors feel this figure is key to the paper, and I want to keep it concise (not a full page). We split the figure into 5 unequal panels to avoid confusion. Now, (a) shows negative vorticity, (b) shows positive vorticity, (c) shows convergence, (d)

shows divergence, and (e) shows SRH. We also added "assuming an eastward-directed storm motion" to the caption for panel (e). [Text and caption wordings also adjusted…]

If necessary, we can make this a single column figure and separate the vorticity and convergence just like we did the SRH from the others. But, hopefully, the new layout and caption explains it sufficiently.

Regarding the authors' response that the mean wind represents an average over a scale of 100 m or less, this is at odds with the body of BL literature. There's actually been a lot of debate in the BL community in just the last few years about the appropriate averaging length/time scales (e.g., Pan and Patton 2017, JTech, "On Determining Stationary Periods within Time Series", and references therein). A 30-min average is probably most commonly used (for time series tower obs). For a 5 m s^{-1} wind, a 30-min average would imply a 9-km horizontal length scale. I am not saying that horizontal surface heterogeneity does not lead to BL wind heterogeneity, but it would strengthen the paper to be clearer about differences between mean and instantaneous winds, and the length scales of heterogeneity that matter. It's easy to forget that the real atmosphere is turbulent when looking at dual-Doppler wind syntheses and model output, which usually smooth and/or don't resolve the turbulence.

There may be a misunderstanding here. It is true that the log wind profile is not strictly applicable over a distance as short as 100 m in the streamwise direction. It shows the profile of the mean wind, averaged over 15–30 min. In this case, we are using the log wind profile as an idealized model to demonstrate [that] the wind heterogeneity that is produced by variations in z_0. There would be a departure from the log wind profile, especially near streamwise gradients in z_0, where internal BL's form and the wind eventually adjusts to a new log wind profile. However, the qualitative aspects of SL convergence and vorticity are still determined by z_0. The length scales of z_0 heterogeneity that matter is still an unresolved issue, but variations on sub-kilometer scales are important, based on Doppler radar observations (including those shown in Fig. 6). This is a topic of future research that is beyond the scope of this paper.

Either way, we made sure to say "the logarithmic wind profile is a good approximation of the profile of the mean wind in a SL with neutral stability". And now we added [elaborating text] in section 3a.

I don't understand response [related to overlake flow and vorticity]. If the near-surface shear upstream of the lake is aligned with the near-surface wind, as it typically is, then the near-surface horizontal vorticity is orthogonal to the long axis of the lake, along which the wind is blowing. If there are dual lake breezes, which seems to be the case from the perturbation winds showing onshore flow on both of the long flanks of the lake, then there'd be a *w* minimum over the lake axis and *w* maxima flanking the *w* minimum. Tilting of the upstream vorticity by this *w* field would result in cyclonic (anticyclonic) ζ on the left (right) flank of the lake, as Fig. 6 shows. I am describing tilting of the upstream ambient near-surface horizontal vorticity, not baroclinically generated vorticity. The tilting of the latter would be tiny because most of it would be along the along-stream flanks of the lake, and therefore aligned with, not orthogonal to, the *w* isotachs. My only point here is that there seems to be an alternative hypothesis that is viable and has not been refuted. *[Editor's Note: This is a potentially important confounding factor in the overlake-flow scenario that the authors should acknowledge and discuss as an alternative possibility, unless they have the data and analyses to refute it.]*

This makes sense now that you clarify it. We thought you were referring to tilting of baroclinic vorticity. But you are referring to tilting of upstream shear by the lake breeze. In the case presented in Fig. 6, we don't know the magnitude of the wind shear upstream of the lake, so determining the magnitude of the tilting term is not doable.

On several of our 13 HRRR simulations where we examined wind speed around the lake vs. wind speed over the lake (section 5c), and the wind speed over the lake was always higher (resulting in the vorticity pattern shown in Fig. 6), the HRRR indicated that the 2-m temperature over the lake was actually warmer than the surrounding land, due to it being cold season, or at night. However, the wind speed was always higher over the lake. The process you describe possibly could enhance (weaken) the vorticity couplet on each side of the lake when there is a lake (land) breeze, but using HRRR 2-m temps, there was no such correlation found. If anything, the acceleration of wind over the lake was greater when the lake was

warmer than the land, perhaps because of relatively small sample size, and several cases were in the cold season. Given that HRRR 2-m temps over the lake may not always be representative, we will mention the concept you bring up in Section 4ai. These results are shown below.

Time	dT (lake)	dspd (kt)
5/11/20 23Z	0	2
12/01/20 00Z	1.5	7
1/18/20 01Z	2	5
2/26/20 15Z	1.5	1
4/30/20 08Z	2	8
4/23/20 03Z	1.5	5
5/11/20 23Z	0	2
5/26/20 20Z	0	4
7/10/20 22Z	-1	1
10/29/20 04Z	1	4
1/19/20 11Z	2	7
1/23/20 18Z	0	2
2/6/20 21Z	0	2

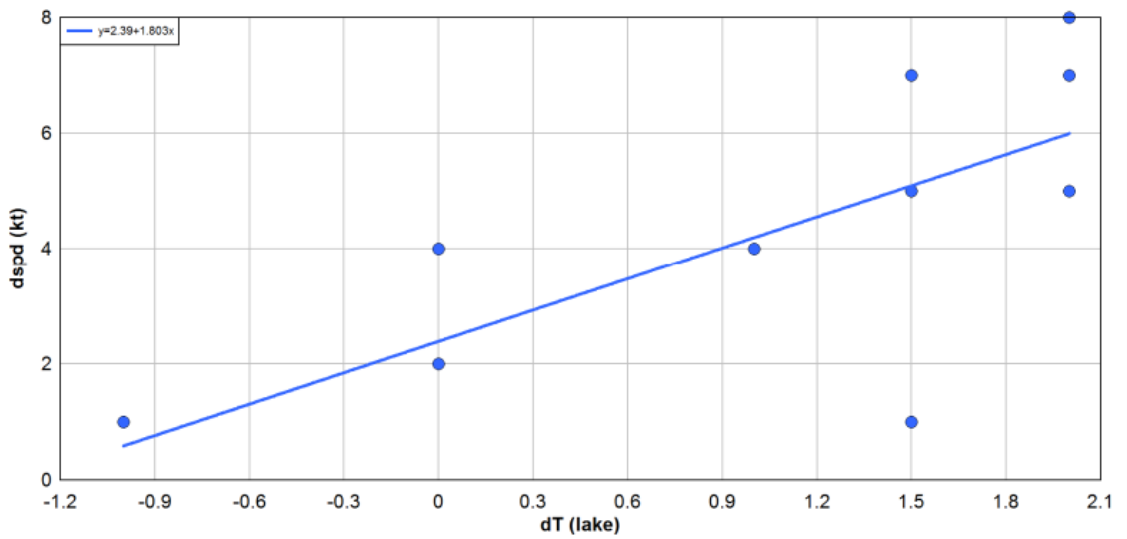

[Minor comments omitted…]

REVIEWER B (Brett J. Roberts):

Initial Review:

Recommendation: Accept with major revisions.

Synopsis: The authors present an overview of how surface roughness length affects PBL wind profiles/vertical shear, and how horizontal heterogeneity thereof can in turn modulate kinematic divergence and vorticity. The illustrations and arguments are directed toward potential impacts on severe convective storms, but the manuscript does not actually evaluate or simulate such impacts explicitly (aside from some calculations of vertical wind shear and SRH); this is left for future work. Thus, I view this manuscript as something like a hybrid short review article and extended introduction to the authors' more substantive

future work. In that capacity, I find the manuscript does a serviceable job with some notable shortcomings. Various studies over the past decade suggest the linkages between PBL kinematics and their underlying land surface properties—rudimentary as these linkages may be qualitatively—were probably undervalued in earlier literature on the dynamics and climatology of severe local storms. Given this history, I see value in presenting clear, concise examples in the style of this manuscript, if only as a convenient reference point for the severe storms research community and operational meteorologists.

I have some comments of substance that approach major status, along with further technical and formatting comments. Given both, I would like to see the manuscript after the first round of revisions.

Dr. Roberts: Thanks for your in-depth review of our paper! It was very helpful, and we appreciate the time you put into it. We answer your comments individually below, and made the associated changes to the manuscript.

Re: Fig. 2 schematic: This schematic strikes me as core to the overall purpose of this manuscript, but is not really discussed in the text; furthermore, even the caption does not quite do it justice. I think it may be important to display a low-level force balance diagram with PGF, Coriolis, and friction corresponding to each land surface in each of (a), (b), and (c). For example, one would not typically expect the wind direction to be identical between the blue and green surfaces in (a) and (b) given an identical geostrophic wind, so you are in a sense assuming offsetting differences in the geostrophic wind for the two surfaces (you make this very point in Section 3c). Furthermore, in (c), there are implicit assumptions about the vertical wind profile that probably need to be made explicit to justify why the vectors drawn imply "low SRH" and "high SRH." Finally, the statement at the end of the caption about storm intensification and rotation should either be removed or modified to say the right panel may conditionally favor intensification of cyclonically rotating updrafts. While much of this may seem pedantic, I come back to the crucial importance of this figure and the likelihood that some people may reference it without even reading the manuscript.

We agree that this figure is a very important piece of the paper…it was a late add! One of the other reviewers thought any force diagrams are too pedestrian for this paper, so we're balancing that reviewer with you (who we agree with). However, we have overhauled Fig. 2 and made it more straightforward. [Editor's Note: Panel description omitted in review section. See caption.] We explain the new figure in the caption, simplify the color scheme, and removed the statement at the end of the caption regarding storm intensity, etc. We also changed our discussion of the figure in the beginning of Section 3. Thanks for your help.

Kelvin's Circulation Theorem states that circulation is conserved about a material circuit in a barotropic fluid in the presence of conservative body forces. In this manuscript, you are mainly talking about near-ground circuits over rough surfaces, so Kelvin's Circulation Theorem is not likely to apply to even a rough approximation most of the time. When you discuss situations like flow along the Florida coastline on p. 12, much of the circulation you are interested in has been generated precisely because of the frictional force operating outside the constraints of Kelvin's Circulation Theorem.

From my perspective, there is a legitimate point buried in the muddy presentation: at time scales on the order of seconds to a few minutes, a material circuit with existing frictionally-generated circulation could experience intense convergence in a supercell, and the convergence could amplify existing vorticity much faster than new frictional vorticity is generated. In that specific scenario, one might argue Kelvin's Circulation Theorem applies to a useful approximation. This just needs to be stated much more clearly to avoid badly misleading naive readers. Please state the relevant caveats when you introduce the theorem, and at some point specify that when you talk about conserving circulation during convergence in severe local storms, it is only in a very approximate sense during extreme convergence (where the convergent augmentation of ambient vorticity is happening much faster than the frictional generation over terrain, for example).

You make an excellent point. We like the term "useful approximation". We have adjusted the wording, per your suggestions. [Also,] in some of Coleman's research, the negative circulation in easterly flow along

the Gulf Coast has weakened the vorticity in supercells moving onshore in some tropical cyclones. We are really just trying to get to the point of conservation of angular momentum.

There are two caveats I'd like to see added to this [section 4b] discussion:

1. The number of times (12) at which SRH could be calculated for UAH and HSV is quite small, so although it is worth presenting the scatterplot, you should explicitly state the limitations of such a small sample size.

2. SPC mesoanalysis is generated on a 40-km grid, so differences on spatial scales of a few km or less as you are interested in have no hope of being resolved. In other words, there may be meteorological factors other than surface roughness playing meaningful roles in subgrid-scale SRH differences in the real world at any given time, even if you have selected times without obvious influences like ongoing convection. Please state this caveat clearly.

Good point, and stated in the text... [Quoted wording omitted].

Re: Circuits and circulation in HRRR output: I am a bit confused about the "8 km circle" passage at the bottom left of p. 12. Is this a horizontal circle? If so, 8-km radius or diameter? Is it at 10 m AGL? More importantly, simply reporting its circulation at one time does not provide any meaningful information to the reader, in my view. How much of the 40000 m^2 s^{-1} was generated frictionally over what period of time? Assuming you don't have access to sub-minute HRRR output to answer this, I would advocate simply removing this entire paragraph. There is an equivalent passage in section 5b about a different circuit to which the same critique would apply. Please remove mention of circulation there, as it is not meaningful without defining the circuit about which it is calculated and analyzing how it was generated.

Paragraph at bottom of page 12 removed. Mention of circulation removed in 5b also. Most readers would not be familiar with magnitudes of circulation at any radius.

[Minor comments omitted…]

Second Review:

Recommendation: Accept with minor revision.

Synopsis: The authors have done a good job of addressing most of my initial comments. I have very minor comments below regarding two changes that were made in response to my initial review, but do not need to see the paper again unless the editor deems it necessary. I will also defer to the editor on my suggestion of replacing "surface wind" with "10 m AGL wind" throughout the paper. Congratulations to the authors on this useful addition to EJSSM!

Dr. Roberts: Thanks for your compliments, and for your in-depth reviews of our paper, that certainly made it better!

REVIEWER C (Jeffrey W. Frame):

Initial Review:

Recommendation: Accept with major revisions.

General Comments: This manuscript describes the meso- and misoscale gradients in wind speed that occur owing to horizontal gradients in surface roughness that lead to areas of enhanced convergence, divergence, and vorticity. These are postulated to potentially influence tornadogenesis, but the discussion and proof of this is left for future work. I think the results described in the manuscript are interesting and deserve to be published in some form. That said, I have two major and several minor comments that I

believe must be addressed prior to formal publication. My chief concerns are that some of the results described in this paper are presented as completely new and novel, which they are generally not, and thus should be described in proper context of previous studies. My second concern is that many the results seem to stem from a couple brief snapshots of observational data and/or model output. To form more robust conclusions, I believe that a longer sample size (possibly up to and approaching a climatology) should be used to draw these conclusions. There are also several explanations that require further clarification or additional discussion that are listed in the minor comments. More details follow below.

Major Comments: In sections 3b and 4, theory and data are presented that document maxima and minima in the divergence and vertical vorticity fields that form owing to the flow of air over a small body of water. It is shown that divergence occurs on the upwind shore, convergence occurs on the downwind shore, positive vertical vorticity develops on the left side of the body of water relative to the wind vector, and negative vertical vorticity forms on the right side. In the manuscript, these are presented as new and novel results, but have been known to, for example, lake-effect snow forecasters even prior to the OWLeS project, although additional data collected during that project further proved their existence. Divergence on the upwind shore and convergence on the downwind shore of a lake has been shown by, for example, Tripoli (2005) and, more recently, Kristovich et al. (2018). The development of lake- and land-breeze fronts and corresponding bands of cyclonic or anticyclonic vorticity along the wind-parallel shores has been shown by, for example, Bergmeier et al. (2017), Steenburgh and Campbell (2017), and in the conference presentation by Miller and Frame (2019). These ideas are also present in textbooks that discuss lake-effect processes both at the introductory (e.g., Rauber et al. 2019) and advanced (Markowski and Richardson 2010) levels. While it is interesting that such features are documented near a lake with spatial dimensions at least an order of magnitude smaller than the more extensively studied Great Lakes, these features should not be treated as new and novel in either the theoretical or observational discussions.

Similarly, the demonstration that the winds in tropical cyclones are stronger over water than over land in section 4aii is also common knowledge to anyone familiar with tropical cyclones and is discussed in introductory meteorology textbooks (e.g., Ahrens and Henson 2017; Rauber et al. 2019).

It was not our intention to present the ideas of air flowing faster over water than land, nor divergence/convergence/vorticity at boundaries of z_0, etc., as novel. We state in section 1 that "In some ways the paper acts as a review of well-established kinematic principles…" However, many scientists, and especially operational meteorologists, are either not aware of these effects, or have not thought of them in terms of severe weather effects. However, to make the point clearer, give the reader more background, and hopefully address your concern, we added references to Welsh (2016); Kristovich et al. 2018; textbook by Rauber et al. 2019; and Minder et al. 2020 in section 3b.

Many of the analyses presented in the manuscript are limited to only specific times whereas I believe the arguments presented would be much stronger if they were substantiated by data or model output over longer periods of time. For example, in section 4aii, the well-known idea that tropical cyclones produce stronger winds over water than they do over land for the same pressure gradient is backed up by only one hour of model output from one storm. There are similar problems with the arguments made in sections 5a and 5b. The upper-air data presented in section 4b considers only two hours' worth of data. Finally, the model output presented in sections 5c and 5d, which examine ambient winds over surface features not associated with severe weather, should examine a much larger set of simulations than a couple of hours on a couple of days. For example, what would happen if the HRRR wind speeds in the vicinity of Lake Wheeler were averaged over an entire month? Or an entire year? A similar methodology should be employed for the gradient in surface roughness near the eastern edge of the Ozark Plateau in Arkansas, rather than examining snapshots of two individual hours, which does not really prove anything. The observations and model output from the Arkansas cases must also be more closely examined for differences in the horizontal pressure gradient. Including a longer period in the study, however, means that this is not necessary.

We have talked to the editor about your concerns here, and he and I agreed on a solution to address your concerns within a timely manner.

We identified 13 cases from 2020 with roughly down-lake or up-lake flow over Lake Wheeler (using KMSL 1-minute ASOS data as initial guess, wind direction between 300° and 340° or 100° and 140°, average hourly speeds >4 m s^{-1}, then using HRRR data, new explaining in section 2), and did a review of those as a short climatology of the winds over Lake Wheeler in both lake-breeze and land-breeze situations (Spring and Summer months when the water is cooler, and autumn and winter months when the water is warmer, in both cases relative to the land.). The results from this study do give a more comprehensive dataset with more credibility, showing indeed that the difference in friction from water to land, in different stability/wind direction/thermal circulation regimes, causes the enhanced wind speeds over the lake and associated vertical vorticity. The results (new Fig. 13b) show HRRR 10-m winds over the lake were always stronger, average 42% stronger, 1.7 m s^{-1} bigger. Also, in each case, positive (negative) vorticity was produced to the left (right) of the wind vector.

[Minor comments omitted…]

Second Review:

Recommendation: Accept with minor revisions.

General Comments: I want to commend the authors on their hard work expanding the sample sizes of both observational and numerical simulation data to better substantiate their conclusions. I also believe that the revised manuscript better presents the results in the context of previously published literature, providing a nice summary of new and existing findings on how differential surface roughness can cause variations in vertical wind shear and SRH. There are only a few remaining minor scientific issues to be addressed, along some additional grammatical errors prior to publication.

Dr. Frame: Thanks for your compliments, and extremely in-depth reviews of our paper and the time you put in. We answer your comments individually below, and made the associated changes to the manuscript. The manuscript is much better now, thanks to all 3 reviews, but as I said before, primarily thanks to yours.

[Minor comments omitted…]